LAWRENCE
LIVERMORE
NATIONAL
LABORATORY

UCRL-TR-221759

Neutron Induced Cross Sections for Radiochemistry for Isotopes of Nickel, Copper, and Zinc

K. Kelley, R.D. Hoffman, F.S. Dietrich, M. Mustafa

June 1, 2006

This work was performed under the auspices of the U.S. Department of Energy by University of California, Lawrence Livermore National Laboratory under Contract W-7405-Eng-48.

UCRL-TR-221759

Neutron Induced Cross Sections for Radiochemistry for Isotopes of Nickel, Copper, and Zinc

K. Kelley, R. D. Hoffman, and F. S. Dietrich
Nuclear Theory and Modeling Group
Physics and Advanced Technologies, N-Division
Lawrence Livermore National Laboratory
Livermore, CA 94550
kelley24@llnl.gov

M. Mustafa
Nuclear and Defense Technologies, AX-Division
Lawrence Livermore National Laboratory
Livermore, CA 94550

June 2, 2006

ABSTRACT

We have developed a set of modeled neutron induced cross sections for use in radiochemical diagnostics. Local systematics for the input parameters required by the Hauser-Feshbach statistical model were developed and used to calculate neutron induced nuclear reaction cross sections for target isotopes of nickel, copper, and zinc ($28 \leq Z \leq 30$) for neutron numbers $30 \leq N \leq 40$.

Subject headings: Nuclear cross sections, Radiochemistry, Nuclear Physics

1. Introduction

1.1. Radiochemistry

Various aspects of nuclear explosive device performance can be determined through the use of radiochemistry. During the UGT (Under Ground Test) Program, select naturally occurring elements were included prior to a test and their activation products subsequently retrieved for counting, typically with gamma-ray detectors. The products were measured as isotopic ratios, such as $^{87}Y/^{88}Y$ produced from the stable isotope of the naturally occurring element. From the measured activity and prior knowledge of the amount of loaded detector material, performance aspects could be inferred by comparing the measured isotope ratios with those calculated using particle fluences from one of the design codes and group-averaged cross section sets prepared for this purpose.

This paper develops the first Copper cross section set for the LLNL RADCHEM library (Nethaway 1998). In previous efforts we have performed similar analysis for several other neutron and/or charged particle detector sets, including ^{79}Br producing ^{79}Kr (Hoffman *et al.* 2004a), ^{127}I producing ^{127}Xe (Hoffman *et al.* 2004b), stable europium producing $^{147-150,152,154}$Eu and ^{151,153}Gd (Hoffman *et al.* 2004c), natural titanium producing ^{48}V or $^{46-48}$Sc, stable ^{52}Cr producing ^{52g}Mn, stable ^{54}Fe producing ^{52g}Mn (Kelley *et al.* 2005), and stable ^{75}As producing ^{73,74}As (Kelley *et al.* 2006). This paper details the unclassified cross section modeling effort.

Contents

List of Figures

List of Tables

1.2. Proposed Cu Detector Set

We consider as targets isotopes of nickel, copper, and zinc with neutron numbers $30 \leq N \leq 40$. This includes any long-lived isomers with half-lives greater than 1 μs. We have calculated nuclear reaction cross sections with incident neutron energies (in the laboratory frame) ranging from 0.01 keV to 20 MeV using the STAPRE Hauser-Feshbach code (Avrigeanu & Avrigeanu 1976). The reaction channels studied include (n,γ), (n,n'), (n,2n), (n,3n), (n,p), (n,np), (n,α), (n,nα), and (n,d). For outgoing channels consisting of two non-identical particles, we combine the modeled cross sections for both orderings of the outgoing particles. For example, reactions listed as (n,np) are in fact the sum of the modeled (n,np) and (n,pn) reactions.

Our goal is to develop a consistent set that reproduces, as closely as possible, measured cross sections on targets in the *local region of interest*. To do this we develop *local systematics* for the many input quantities used in the theoretical reaction modeling calculations. These systematics are based on experimental data that are often only available for compound nuclear systems formed from a stable target plus a neutron. Of course, we use experimental data whenever it is available, but reactions proceeding through unstable systems are unavoidable in radiochemistry. Short of developing new experimental techniques to measure cross sections on radioactive targets, our only hope is to develop theory cross section sets that reproduce measurements in the region of interest without tuning model input parameters for individual nuclei.

The theoretical techniques embodied by the STAPRE-H95 code used in our modeling effort, including the Hauser-Feshbach model, width fluctuation correlations, and the exciton preequilibirium model, have been thoroughly documented in previous reports (Hoffman *et al.* 2004a-c; Kelley *et al.* 2005,2006) and will not be repeated here. In §2 we present the input parameters used in our modeling effort and detail the development of systematics for level density parameters and gamma ray transmission coefficient normalizations. In §3 we give our results. Conclusions follow in §4.

2. Inputs Required for the Hauser-Feshbach Model

2.1. Nuclear Structure Data

2.1.1. Nuclear Masses and J^π Assignments

We adopt the experimental mass excess values of (Wapstra Audi & Thibault 2003). Spin and parity assignments are from (ENSDF 2003). We present in Table 2 (Appendix A.1) the binding energy (in MeV) calculated from the adopted mass for the ground states and isomers of each isotope included in this study. Additionally we list the spin and parity assignments and particle separation energies for each exit channel considered. Note that for isomer targets the binding and separation energies are reduced by the isomer energy, given in parenthesis in table A.1. In Table 3 (Appendix A.2), we provide reaction Q-values for the cross sections studied in this report.

2.1.2. Nuclear Level Schemes

The nuclear structure data needed to model the gamma-ray cascade in this study was adopted from (Belgya *et al.* 2005). The number of excited levels adopted for each nucleus is given as the quantity "N" in Table 4 (Appendix A.3). Generally, this is the number for which energy spin and parity are unambiguously assigned. Nuclei for which only a ground state was used are indicated by N=0.

2.2. Transmission Coefficients

2.2.1. Neutron and Proton Optical Potentials

For the calculation of the neutron and proton particle transmission coefficients, we use the optical model of (Koning & Delaroche 2003). Although they have tuned their parameters to fit data for many different species (see their Tables 6 and 7), we decided to use the global nucleon-nucleon optical model potential (OMP), as it gives a satisfactory fit to measured total cross section data for neutrons and protons in the range of interest to us. Specifically, we adopt the potential depth parameters and Fermi energies for the neutron and proton global OMP defined in their Section 5.2, tables 14 and 15. The particle transmission coefficients were generated by the optical model code ECIS-95 (Raynal 1996). Although designed for coupled channel calculations, we used the code in a spherical optical model mode.

This optical model has produced favorable comparisons to measured total neutron cross sections

in the regions of scandium, titanium, vanadium, chromium, manganese, and iron (Kelley *et al.* 2005), arsenic (Kelley *et al.* 2006), bromine and krypton (Hoffman *et al.* 2004a), and iodine and xenon (Hoffman *et al.* 2004b). Additionally, comparisons made in (Koning & Delaroche 2003) indicate that this optical potential does very well in replicating total cross sections, differential elastic cross sections, and analysing power measurements for both incident neutrons and protons.

2.2.2. The Alpha and Deuteron Optical Potentials

We have included possible alpha and deuteron exit channels in this modeling effort. For the alpha particles, we use the optical potential of (Avrigeanu *et al.* 1994), and for deuterons we use that of (Lohr & Haeberli 1974), as encoded in the SCAT2 subroutine of STAPRE-H95.

We do not include a quality analysis of these potentials in this report. The deuteron and alpha exit channels are generally small when compared to the dominant channel, and any sensitivity to these optical potentials will only be apparent in the weak exit channels. Additionally, somewhat reasonable agreement with the experimental (n,α) cross sections provides us with a degree of confidence in the alpha potential (see Figure 8).

2.2.3. Transmission Coefficients for Photons

For the calculation of the gamma ray transmission coefficients, we use a simple model where the transmission coefficient depends only on the multipole type (XL) and the transition energy (ϵ). They are related to the gamma ray strength function $f^{\gamma}_{XL}(\epsilon)$ by

$$T^{\gamma}_{XL}(\epsilon) = 2\pi\epsilon^{2L+1} f^{\gamma}_{XL}(\epsilon) \qquad (1)$$

The energy dependence of the strength function was determined using the GDR model with simple Lorentzian line shapes. In particular, the E1 strength function is given by

$$f^{\gamma}_{E1}(\epsilon) = \mathcal{N}\zeta\sigma_G \frac{\Gamma_G^2\epsilon}{\left(\epsilon^2 - E_G^2\right)^2 + \left(\Gamma_G\epsilon\right)^2} \ (\mathrm{MeV}^{-3}) \quad (2)$$

where E_G, Γ_G, and σ_G are the energy, width, and peak cross section of the giant dipole resonance given in MeV and mb respectively. The constant ζ is 8.674×10^{-8} mb^{-1}·MeV^{-2}. The adopted GDR parameters are given by

$$\begin{aligned} E_G &= \frac{80 \text{ MeV}}{A_C^{1/3}} \\ \Gamma_G &= 5 \text{ MeV} \\ \sigma_G &= A_C \frac{13 \text{ mb}}{5} \end{aligned} \qquad (3)$$

where A_C is the mass number of the compound nucleus. We also include M1, E2, M2, E3 and M3 transitions using Blatt-Weisskopf strength functions

$$\begin{aligned} f^{\gamma}_{M1}(\epsilon) &= 3.1\times10^{-1} A_C^{-2/3} f^{\gamma}_{E1}(S_n) \\ f^{\gamma}_{E2}(\epsilon) &= 7.2\times10^{-7} A_C^{2/3} f^{\gamma}_{E1}(S_n) \\ f^{\gamma}_{M2}(\epsilon) &= 2.2\times10^{-7} f^{\gamma}_{E1}(S_n) \\ f^{\gamma}_{E3}(\epsilon) &= 3.4\times10^{-13} A_C^{4/3} f^{\gamma}_{E1}(S_n) \\ f^{\gamma}_{M3}(\epsilon) &= 1.1\times10^{-13} A_C^{2/3} f^{\gamma}_{E1}(S_n) \end{aligned} \qquad (4)$$

where S_n is the neutron separation energy. Since the strength functions are constants, the transmission coefficients for these transitions are simply proportional to ϵ^{2L+1}.

The factor $\mathcal{N}$ appearing in Eq. 2 is a normalization constant, determined by fitting to the average total s-wave radiation width at the neutron binding energy for the appropriate compound nucleus,

$$\begin{aligned} \langle\Gamma_\gamma\rangle_0 &= \frac{J+1}{2J+1}\left\langle\Gamma_\gamma\left(B_n, J+\frac{1}{2}\right)\right\rangle \\ &+ \frac{J}{2J+1}\left\langle\Gamma_\gamma\left(B_n, J-\frac{1}{2}\right)\right\rangle \end{aligned} \qquad (5)$$

$$\langle\Gamma_\gamma(E,J)\rangle = \frac{T_\gamma(E,J)}{2\pi\rho(E,J)} \ (\mathrm{meV})$$

(Uhl & Strohmaier 1976). Here, J is the spin of the target nucleus. The gamma-ray transmission coefficient appearing in this expression is the total transmission coefficient, including a sum over discrete states and (possibly) an integration with the level density up to the appropriate excitation energy. Since the total s-wave radiation width is generally measured only for stable isotopes plus a neutron, we have developed a systematic approach for estimating this value for the many unstable nuclei in our region of interest. The systematic values are determined by a least squares linear fit to experimental data. Using measured radiation widths for compound nuclei in the range $16 \le Z \le 32$, the linear fit yields

$$\langle\Gamma_\gamma\rangle_0^{\text{sys.}} = -22.8076\times A + 1890.14 \qquad (6)$$

This fit is shown in Figure 1. Note that many of the measured radiation widths for elements up through nickel have very large errors. We have

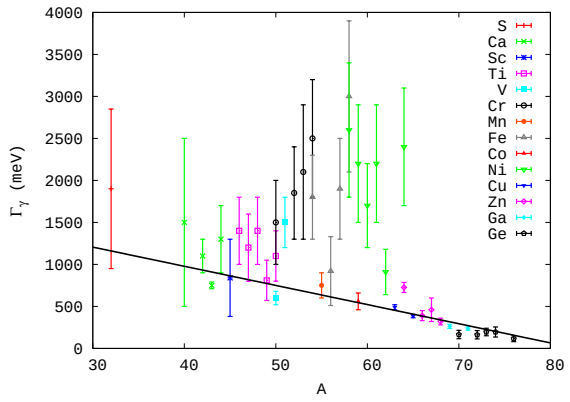

Fig. 1.— Least squares linear fit to measured $\langle\Gamma_\gamma\rangle_0$ in the region of interest. The measured data is taken from (Belgya *et al.* 2005), and our systematic is represented by the solid black line.

found that using these measured widths generally results in an overestimation of modeled capture cross sections. The radiation widths predicted by our systematic produces results in much better agreement with experimental cross section data. Thus, we adopt only the systematic values in our modeling effort.

2.3. Nuclear Level Densities

Another important input to the statistical model code is the nuclear level density. For this project, we have adopted a standardized, semi-empirical approach which is numerically efficient and can be tied to experimental data. The level density is described by two functions

$$\rho\left(U,J\right)=\rho\left(U\right)f\left(U,J\right) \tag{7}$$

Both are energy dependent, the second factor contains the spin dependence. In this expression, $\rho(U)$ is the state density, $U=E-\Delta$ is the backshifted energy (Δ is the so-called "backshift"), and J is the spin of the compound nucleus. We will further treat each component of Eq. 7 in two ways, depending on the excitation energy of interest. The demarcation point will be roughly between the energy range of the known excited levels of a given compound nucleus (the low energy domain), and near the neutron binding energy (the high energy domain).

The process of developing local systematics for the level density has been thoroughly described in previous papers (Hoffman *et al.* 2004a; Hoffman *et al.* 2004b; Hoffman *et al.* 2004c; Kelley *et al.* 2005; Kelley *et al.* 2006), and we will only touch on the more salient points in the present work. For the high energy domain, we describe the level density assuming a backshifted Fermi gas formula,

$$\rho\left(U\right)=\frac{\sqrt{\pi}}{12}\,\frac{\exp\left(2\sqrt{aU}\right)}{a^{1/4}U^{5/4}}\,\frac{1}{\sqrt{2\pi}\sigma} \tag{8}$$

$$f\left(U,J\right)=\frac{2J+1}{2\sigma^2}\,\exp\left[\frac{-\left(J+\frac{1}{2}\right)^2}{2\sigma^2}\right] \tag{9}$$

where $a(U)$ is the level density parameter (in MeV^{-1}) and U is the backshifted energy given by $U=E-\Delta$ with

$$\begin{aligned}
\Delta(Z,N) &= \frac{\Delta_p+\Delta_n}{2} \\
\Delta_p\left(Z,N\right) &= E^G\left(Z,N\right) \\
&- \frac{1}{2}E^G\left(Z-1,N\right) \\
&- \frac{1}{2}E^G\left(Z+1,N\right) \\
\Delta_n\left(Z,N\right) &= E^G\left(Z,N\right) \\
&- \frac{1}{2}E^G\left(Z,N-1\right) \\
&- \frac{1}{2}E^G\left(Z,N+1\right)
\end{aligned} \tag{10}$$

The various $E^G\left(Z,N\right)$ are binding energies, listed in table 2. The spin cutoff parameter σ^2 appearing in Equations 8 and 9 is defined as

$$\sigma^2=\lambda^2(0.1223)^2A^{5/3}\sqrt{\frac{U}{a}} \tag{11}$$

Here, λ is the ratio of the moment of a rigid deformed nucleus to a rigid sphere of the same mass and volume. The value of λ for a given nucleus can be calculated from the Nilsson model deformation parameters, as given in (Möller *et al.* 1995) (see their section 2.2). We assume a non-axiality angle of zero, which greatly simplifies the calculation of these ratios, which are tabulated in Table 4 of Appendix A.3.

We use an energy dependent level density parameter

$$a(U)=\tilde{a}\left[1+\delta W\frac{f(U)}{U}\right] \tag{12}$$

with $f(U)=1-\exp(-\gamma U)$ (Iljinov *et al.* 1992). The quantity δW is the shell correction, for which we adopt the so-called "microscopic correction" from (Möller *et al.* 1995), in the manner of (Rauscher *et al.* 1997).

For a given Δ and σ^2, the level density parameter $a(U)$ can be related to the average s-wave

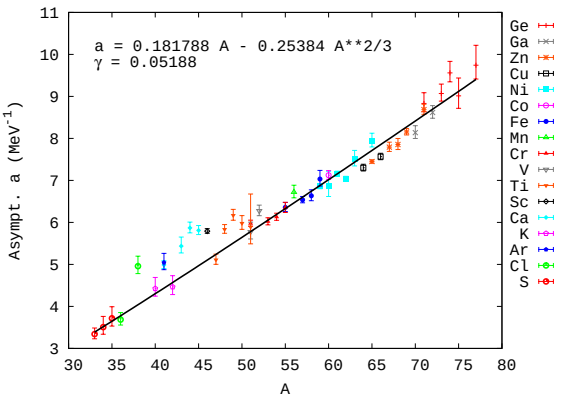

Fig. 2.— Three parameter fit to derived "experimental" asymptotic level density parameters, used to systematically determine unknown $\tilde{a}$. The data are obtained from measured s-wave resonance spacings listed in (Belgya *et al.* 2005), assuming our chosen parameterizations for the backshift and spin cutoff parameter. Our systematic, fit only to the data shown in this figure, is represented by the solid black line.

level spacing at the neutron binding energy (D_0) for nuclei where such quantities are measured. For other nuclei we must develop a systematic description of $a(U)$. We assume that $\tilde{a}$ is of the form $\tilde{a} = \alpha A + \beta A^{2/3}$, similar to (Rauscher *et al.* 1997). Using the relation

$$D_0^{\rm calc} = \frac{2}{\rho\left(U, J = \frac{1}{2}\right)} \tag{13}$$

for nuclei with spin $s = 0$ and

$$D_0^{\rm calc} = \frac{2}{\rho\left(U, J = s + \frac{1}{2}\right) + \rho\left(U, J = s - \frac{1}{2}\right)} \tag{14}$$

for nuclei with $s \neq 0$, we numerically solve for the values of α, β, and γ that minimize the quantity

$$\chi^2 = \sum_i \left(\frac{D_0^{\rm calc} - D_0^{\rm exp}}{\delta D_0^{\rm exp}} \right)^2 \tag{15}$$

where $\delta D_0^{\rm exp}$ is the error in the measured D_0 and the sum is taken over all measured D_0 for target nuclei in the range $16 \leq Z \leq 32$. The resulting fit finds $\alpha = 0.181788$, $\beta = -0.25384$, and $\gamma = 0.05811$, and is shown in Figure 2. When calculating cross sections, we always use the "experimental" $a(U)$, derived from a measured D_0, when they are available.

At low energies, the nuclear level density is better described by a constant temperature formula:

$$\rho(E) = \frac{1}{\sqrt{2\pi}\sigma} \frac{1}{T} \exp\left[\frac{E - E_0}{T}\right] \tag{16}$$

(Gilbert & Cameron 1965). This formula must tangentially match Equation 8 at some energy E_x that lies between Δ and the neutron binding energy. This constraint fixes E_0 and T for a given E_x, and hence E_x may be adjusted to give the best possible fit to low-lying spectroscopic levels. The spin-cutoff parameter σ is assumed to be constant below E_x. Typical values for the matching energy are $2 \leq E_x \leq 8$ MeV, and are approximated by $E_x = 2.5 + \frac{150}{A} + \Delta$ (Gilbert & Cameron 1965).

We define the notion of achieving a "good" fit to the total level density over the entire energy range if (a) a good fit can be made to the low lying levels, (b) the observed level spacing at the neutron binding energy is exactly reproduced, and (c) the energy of the matching point E_x for the two prescriptions falls between $E = \Delta$ and $E = B_n$.

In our attempts to match the the level density to the number of discrete levels, we generally try to ensure that the integrated level density at the energy of the last known level is equal to the cumulative number of known levels. This ensures that the effective level density will be continuous as the Hauser-Feshbach model shifts between the discrete levels and the level density. However, there are cases where matching at the energy of the last discrete level is not possible (i.e. matching would require $E_x < \Delta$ or $T < 0$). Occasionally the resulting lower limit on the matching energy precludes matching the last discrete level, and the integrated level density/cumulative number of levels suffers a discontinuity (recall that the Hauser-Feshbach formula only employs the level density above the energy of the last discrete level). Such discontinuities have been found to result in gross non-physical behavior for some cross sections, particularly (p,n) cross sections. In most of these cases, one can match the integrated level density to the cumulative number of levels by reducing the number of discrete levels included in the calculation. This is the approach we take. In a few instances, even a reduction in the included discrete levels could not fully rectify the situation. For those nuclei, we use the smallest allowable matching energy (with $E_x > \Delta$ and $T > 0$) to reduce the size of the discontinuity as much as possible.

The fitted parameters for the total level density are presented in Table 4 (Appendix A.3). The symbols in the legend are the same as described

above. In column three, an "x" indicates the level density parameter $\tilde{a}$ was derived from an experimentally known level spacing (D_0), an "s" indicates that $\tilde{a}$ was derived from the systematic shown in Figure 2.

2.4. Considerations Regarding the Exciton Pre-Equilibrium Model

We adopt a simple exciton model with initial 2-particle 1-hole configuration. Average rates for internal transitions are given by the formulas of (Williams 1970), corrected for the Pauli principle by (Cline 1972), and are related to the absolute square of the average effective matrix element $|M|$ of the residual interactions as per Eq. (7) of (Uhl & Strohmaier 1976). The dependence of $|M|^2$ on mass number and excitation energy is

$$|M|^2 = \langle FM \rangle A^{-3} E^{-1} \tag{17}$$

The parameter $\langle FM \rangle$ may be tuned to best replicate measured cross section data. For this region, we find that a value of $\langle FM \rangle = 400$ is satisfactory.

When included as a possible exit channel, one should account for alpha particles in the pre-equilibrium phase of the reaction. Generally, the description of alpha particle emission in the exciton model is a straightforward extension of the description of neutron or proton emission. In making such an extension, one introduces a parameter ϕ which represents the probability that the incoming particle will strike a pre-formed alpha cluster (Milazzo-Colli *et al.* 1973). It follows that the larger values of ϕ will result in a higher probability of subsequent alpha emission, thus enhancing the (n,α) reactions. In our calculations, we have chosen a value of $\phi = 0.20$, although previous considerations of alpha emission suggest that this value may fall anywhere in the range of $0.1 \leq \phi \leq 0.8$ within the mass range of interest (Milazzo-Colli *et al.* 1973). We have chosen this value primarily because it results in (n,α) cross sections which best fit the available experimental cross section data. Since the alpha particle emission accounts for a relatively small portion of the total reaction cross section (generally less than 20%), variations in the ϕ parameter will only have minor effects on the other cross sections.

3. Calculated Cross Sections

3.1. Comparison to Measured Cross Sections

We now compare our statistical model cross sections, calculated using the presriptions and systematics described in the previous section, to available measured cross section data in the region of interest.

Figure 3 presents our neutron capture cross sections relative to experimental data in the region of interest. The panels of Figure 3 have been laid out in increasing target charge and mass as one views the figure from the bottom to top or left to right. The data shown is an aggregate of measurements available from (CSISRS 2003). Data at very low energies (generally 10 keV or less) has been omitted, on the basis that at very low incident energies the level spacing in the compound nucleus becomes large, and the effects of individual resonances (which cannot be replicated by the statistical model) are apparent. The grey data points represent measured activation cross sections. Orange and light blue data represent measured cross sections leading to the ground state and first isomer of the residual, respectively. The solid lines (black, red, and blue) represent our calculations (activation, amount to ground state, and amount to first isomer).

Qualitatively, the agreement between our calculations and the measured neutron capture cross sections is quite favorable, with our calculation usually being well within a factor of two of the experimental data. The most notable deviations occur for ^{65}Cu between ~300-1000 keV incident neutron energy and for ^{68}Zn. In the former case, we note that our calculation is still roughly within a factor of two over the energy range in question, and that the cross section is quite small (on the order of 10 millibarns). Nevertheless, the neutron capture cross section is the dominant destruction cross section for ^{65}Cu at low incident energies (see Figure 12 in Appendix B). For the latter case (^{68}Zn), the various data sets appear to be in conflict, i.e. the measured cross sections leading to the ground state and first isomer of the residual do not add up to the measured activation cross section, with the exception of the single activation cross section measurement at ~30 keV. It is likely that our calculation runs high for this reaction, though most likely within at least a factor of three.

An additional evaluation of our calculated neutron capture cross sections can be made by com-

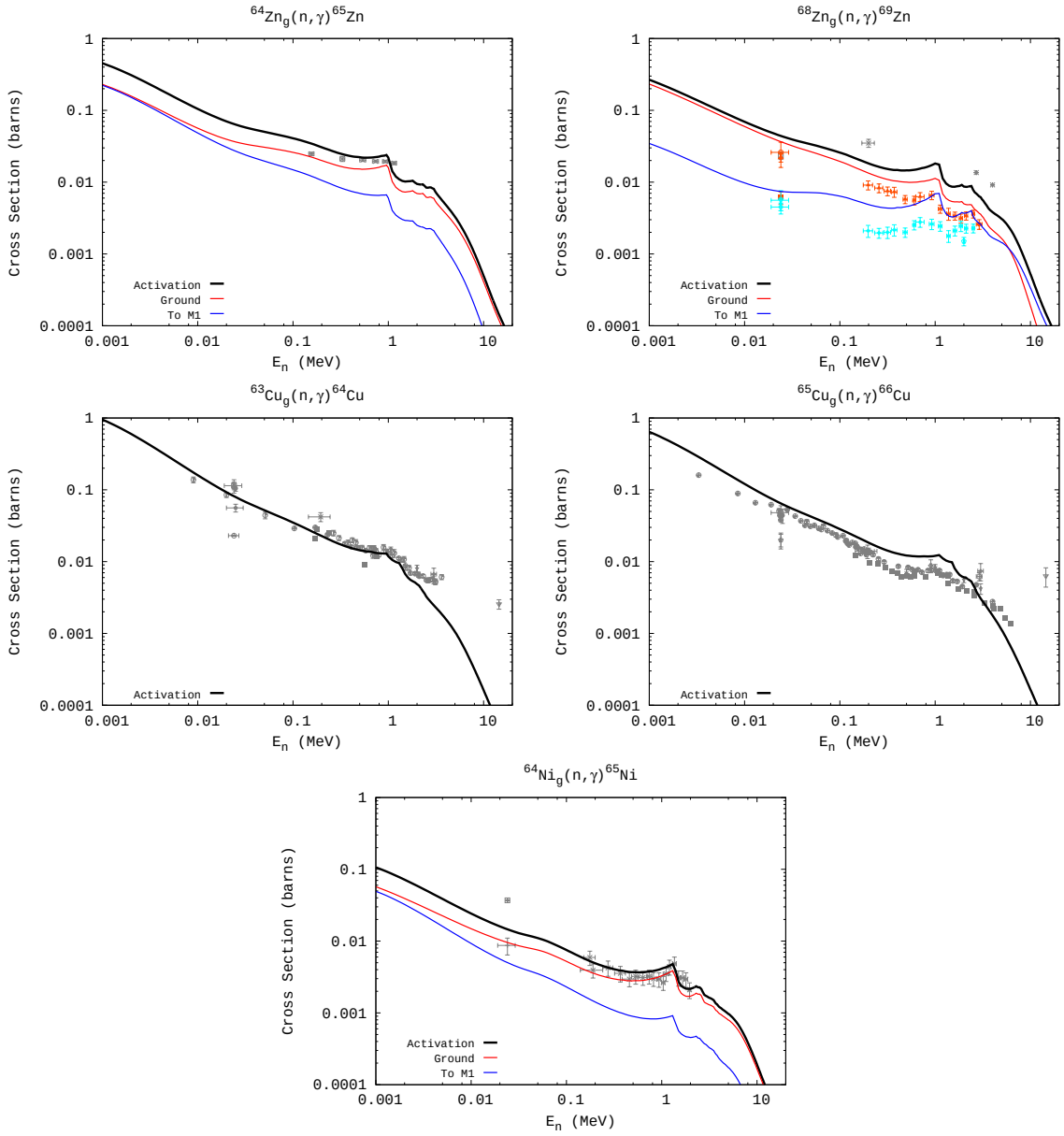

Fig. 3.— Calculated vs. measured neutron capture cross sections on select stable targets of Ni, Cu, and Zn. Measured cross sections are obtained from (CSISRS 2003). The solid black lines and grey data represent activation cross sections. Solid red lines and orange data represent the cross section going to the ground state of the residual (equal to the activation cross section when the residual nucleus does not have an isomer). Blue lines and cyan data represent the cross section going to the first isomer.

paring to a standard set of 30 keV Maxwellian-averaged cross sections (MACS), The MACS is defined as the reaction rate $\langle \sigma v \rangle$ divided by the mean velocity $v_T = \sqrt{2kT/\mu}$ at a given temperature T, with μ the reduced mass. Extensive efforts have been made to evaluate capture MACS for astrophysical applications (Bao *et al.* 2000). For particle fluences and temperatures typical to stellar nucleosynthesis, the velocity distribution of the neutrons reduces to a Maxwell-Boltzmann form. In turn, the MACS reduces to (Beer *et al.* 1992)

$$\frac{\langle \sigma v \rangle}{v_T} = \frac{\int_0^\infty \sigma_{n\gamma} v \Phi(v) dv}{v_T} = \frac{2}{\sqrt{\pi}(kT)^2} \int_0^\infty \sigma_{n\gamma}(E) W(E, kT) dE \quad (18)$$

where $W(E, kT) = E \exp(-E/kT)$ and E is the

center of mass energy. Using spline interpolation to determine the value of the (n,γ) cross section between points on the energy grid, and assuming a $E_{lab}^{-1/2}$ energy dependence below our lowest grid energy, our modeled (n,γ) cross sections yield the MACS presented in Table 1. The recommended values are taken from (Bao *et al.* 2000).

Table 1: Modeled v. recommended 30 keV Maxwellian-averaged neutron capture cross sections

Target	$\langle\sigma v\rangle_{\rm calc}$	$\langle\sigma v\rangle_{\rm exp}$	calc/exp	%Err
^{58}Ni	41±2	22.9	0.559	-44.1
^{59}Ni	87±14	38.3	0.440	-56.0
^{60}Ni	30±3	21.4	0.713	-28.7
^{61}Ni	82±8	33.1	0.404	-59.6
^{62}Ni	12.5±4	18.8	1.504	44.0
^{63}Ni	31±6	28.5	0.919	-8.1
^{64}Ni	8.7±0.9	13.8	1.586	58.6
^{63}Cu	94±10	75.1	0.799	-20.1
^{65}Cu	41±5	59.0	1.439	43.9
^{64}Zn	59±5	64.1	1.086	8.6
^{65}Zn	162±27	168.2	1.038	3.8
^{66}Zn	35±3	52.1	1.489	48.9
^{67}Zn	153±15	130.0	0.850	-15.0
^{68}Zn	19.2±2.4	42.2	2.198	119.8
^{70}Zn	21.5±2.0	32.4	1.507	50.7

These comparisons provide us with a more quantitative evaluation of our neutron capture cross sections. In particular, we note that all of the MACS, with the exceptions of those involving ^{59}Ni and ^{68}Zn targets, are within a factor of two of the recommended values (it should be noted that the recommended MACS for ^{59}Ni, and also ^{63}Ni, are based on theory calculations rather than actual measurements). The result for ^{68}Zn, for which our calculation is high compared to the recommended data by a factor of 2.2, is consistent with the comparison to measured cross sections shown in Figure 3. On average, our calculated MACS are within 40.7% of the recommended values.

Due to their sensitivity to both the level density and gamma ray strength functions, neutron capture cross sections are among the more difficult to model. Using global systematics, (n,γ) cross sections can typically be modeled to within a factor of two, sometimes to within 30% (Hoffman *et al.* 1999).

In Figure 4 we present our modeled (n,n') cross sections compared to measured data. Again, the panels are arranged to show increasing charge and mass as one moves up and to the right on the figure. Only activation cross section data is available from (CSISRS 2003) for (n,n') reactions in this region, with most of the data at or above 14 MeV incident neutron energy. The one exception is ^{63}Cu, for which our calculation compares most favorably to the lower energy data. Above roughly 10 MeV incident energy, non-statistical processes, most notably direct reactions and pre-equilibrium emission, begin to make significant contributions to the inelastic cross section. Our systematic underestimation of the (n,n') cross section above 10 MeV is most likely due to the omission of direct reactions, although inaccuracies in the pre-equilibrium model may also play a role.

Since there are no isomers for any copper isotopes between $A = 58$ and $A = 67$, the (n,n') reaction channels will have no effect in the radiochemical diagnostics of copper. Rather, they serve primarily as a further means of analysing the quality of our statistical model inputs.

The (n,2n) reaction channel is among the most important in radiochemical diagnostics. Usually it is the dominant channel for neutron energies between 10-15 MeV, though (n,np) will sometimes compete. Fortunately, (n,2n) reactions are also among the easier reactions to model, as they scale roughly with the size of the nucleus with the activation cross section typically about 1-1.5 barn at 14 MeV regardless of atomic number in this region of the nuclear chart. In Figure 5 we compare our modeled (n,2n) cross sections to measured data from (CSISRS 2003). The available (n,2n) data in this region of interest generally falls into one of two catagories. It is either quite sparse (consisting of a single data point for ^{60,64}Ni and ^{68}Zn), or quite disparate (as in the cases of ^{58}Ni, ^{63}Cu, and ^{64,70}Zn). This makes an evaluation of our (n,2n) cross sections somewhat more difficult. However, in the cases where there is an abundance of measured data with reasonable consistency (for instance ^{65}Cu or ^{66}Zn) our calculations do quite well. In other cases where the data is abundant but disparate, our modeled cross sections tend to be in good agreement with at least one set of data. In the cases where cross section data is sparse, we tend to run on the high side.

The (n,p) cross sections on stable targets in this region of interest are fairly well measured. We compare our modeled (n,p) cross sections to the available data in Figure 6. The overall agreement is satisfactory, though there are some features worth pointing out. In a few cases (specifically ^{64,66,67}Zn), our modeled cross sections are

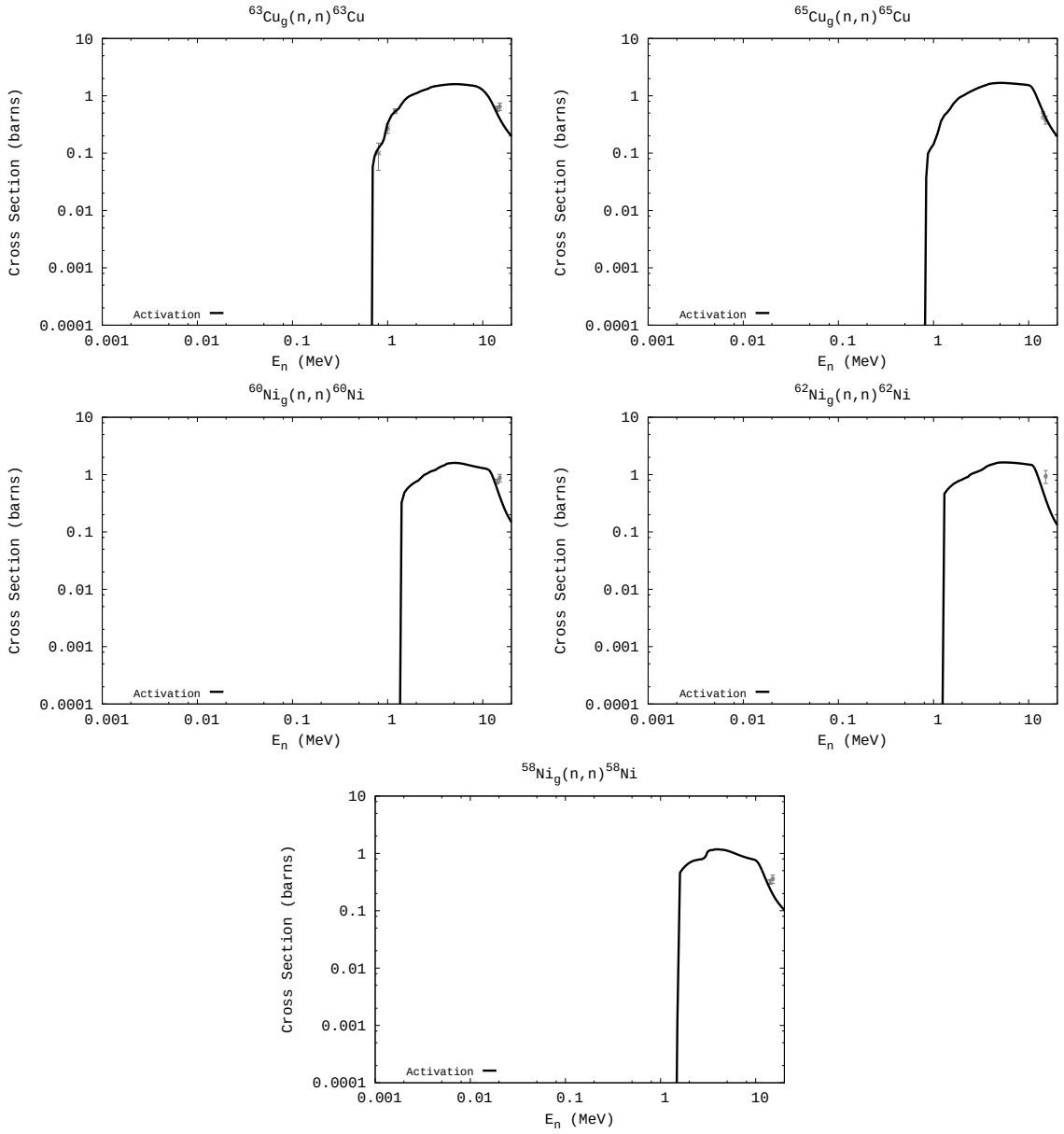

Fig. 4.— Calculated vs. measured (n,n') cross sections on select stable targets of Ni, Cu, and Zn. Measured cross sections are obtained from (CSISRS 2003). The solid black lines and grey data represent activation cross sections. Solid red lines and orange data represent the cross section going to the ground state of the residual (equal to the activation cross section when the residual nucleus does not have an isomer). Blue lines and cyan data represent the cross section going to the first isomer.

high on the rise from threshold. This appears only to be the case with zinc targets. Also, for ^{65}Cu the peak of our modeled cross section appears to be high by as much as a factor of two, although there is quite a bit of variance in the measured data at the peak. The agreement between our calculations and experimental (n,p) cross sections are quite favorable for the nickel targets.

We note that the (n,p) channel is generally small compared to the dominant channel above 10 MeV in this region, and typically smaller than the neutron capture channel at low incident energies. However, it is usually the dominant neutron channel between ∼2-10 MeV (see Figure 12, Appendix B), and hence it is desireable that the modeled (n,p) cross sections be as accurate as possible over this energy range. There are also cases

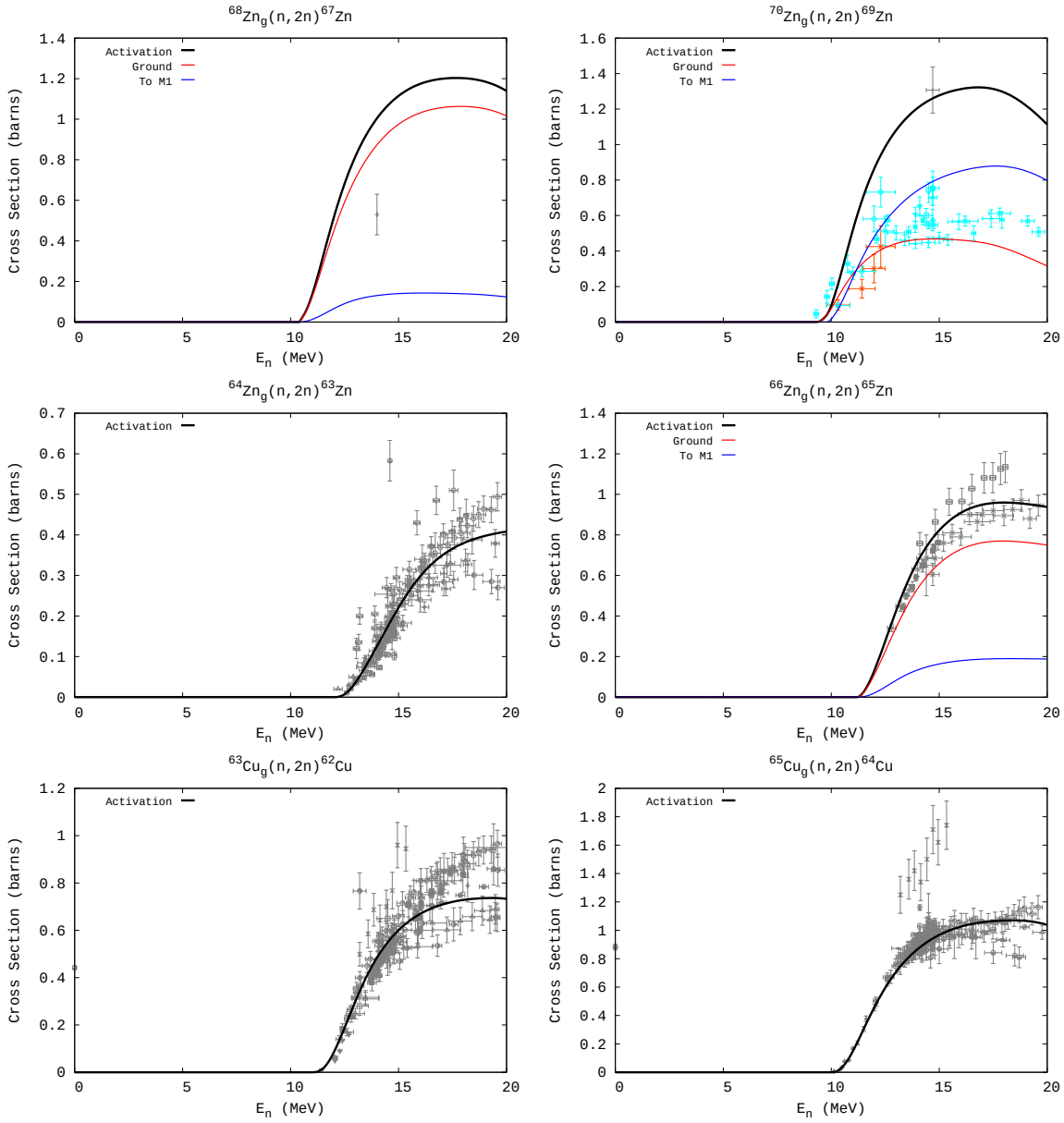

Fig. 5.— Calculated vs. measured (n,2n) cross sections on select stable targets of Ni, Cu, and Zn. Measured cross sections are obtained from (CSISRS 2003). The solid black lines and grey data represent activation cross sections. Solid red lines and orange data represent the cross section going to the ground state of the residual (equal to the activation cross section when the residual nucleus does not have an isomer). Blue lines and cyan data represent the cross section going to the first isomer.

where (n,p) dominates significantly over neutron capture at low energies. This is particularly the case for proton rich targets. The (n,p) channel is quite significant for ^{63,64}Cu targets.

Next to (n,2n), the (n,np) reaction is among the more important reaction channels above 10 MeV, at times being larger than (n,2n) (see Figure 12 in Appendix B, particularly for proton rich targets). Unfortunately, relatively few (n,np) measurements have been made in this region. Figure 7 compares our calculations to the available measured cross section data. Because the data is sparse, and at times quite disparate (^{63}Cu), with large errors (^{65}Cu), or lying primarily just above threshold, a definitive analysis of our modeled (n,np) cross sections is difficult. In the most well measured case, ^{58}Ni, our calculation appears to be high by roughly

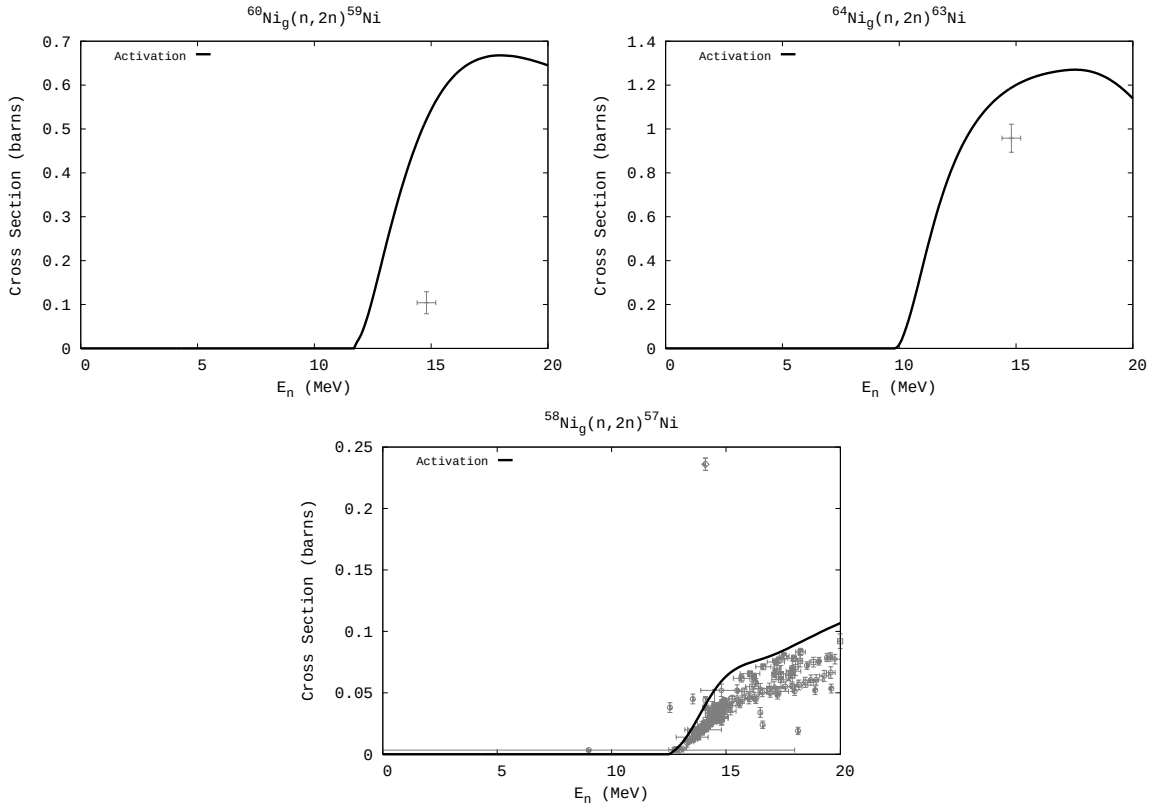

Fig. 5.— (continued)

15%.

The agreement between our modeled (n,α) cross sections and measurement, presented in Figure 8, is similar to that encountered with the (n,p) reactions. We note that the (n,α) cross section is almost always quite small compared with the dominant channel at any given incident energy, and its effect should be of minor importance to UGT analysis. However, (n,α) cross sections do provide us an additional means of evaluating the quality of our statistical model input parameters, particularly the alpha particle transmission coefficients.

In Figure 9 we compare our modeled (n,nα) cross sections to the available data from (CSISRS 2003). In the two more well-measured cases (^{65}Cu, ^{70}Zn), our calculation compares quite favorably to the data. We note that this channel is always small compared to the dominant channel, as is the (n,d) channel presented in Figure 10.

Overall, we consider our modeling effort to be quite successful in reproducing measured neutron induced cross sections in this region of interest. We have also calculated several charged particle induced cross sections on these same targets and found similar favorable results.

3.2. Sensitivity Studies

In prior reaction modeling efforts, we have thoroughly investigated the sensitivity of Hauser Feshbach calculations to variations in the many input parameters (Hoffman *et al.* 2004a; Hoffman *et al.* 2004b; Hoffman *et al.* 2004c; Kelley *et al.* 2005; Kelley *et al.* 2006). We have not made an extensive effort to study the sensitivities of the cross sections in this report to such variations, but contend that the results would be similar to those found in other nearby local regions (see Kelley *et al.* 2005; Kelley *et al.* 2006).

3.3. Production and Destruction Cross Sections

Figure 11 shows the modeled cross sections that directly affect the production and destruction of ^{64}Cu. Identical plots for each of the ground state targets considered in this study are presented in Appendix B.

Since we are considering only neutron induced reactions, the capture and (n,2n) cross sections are

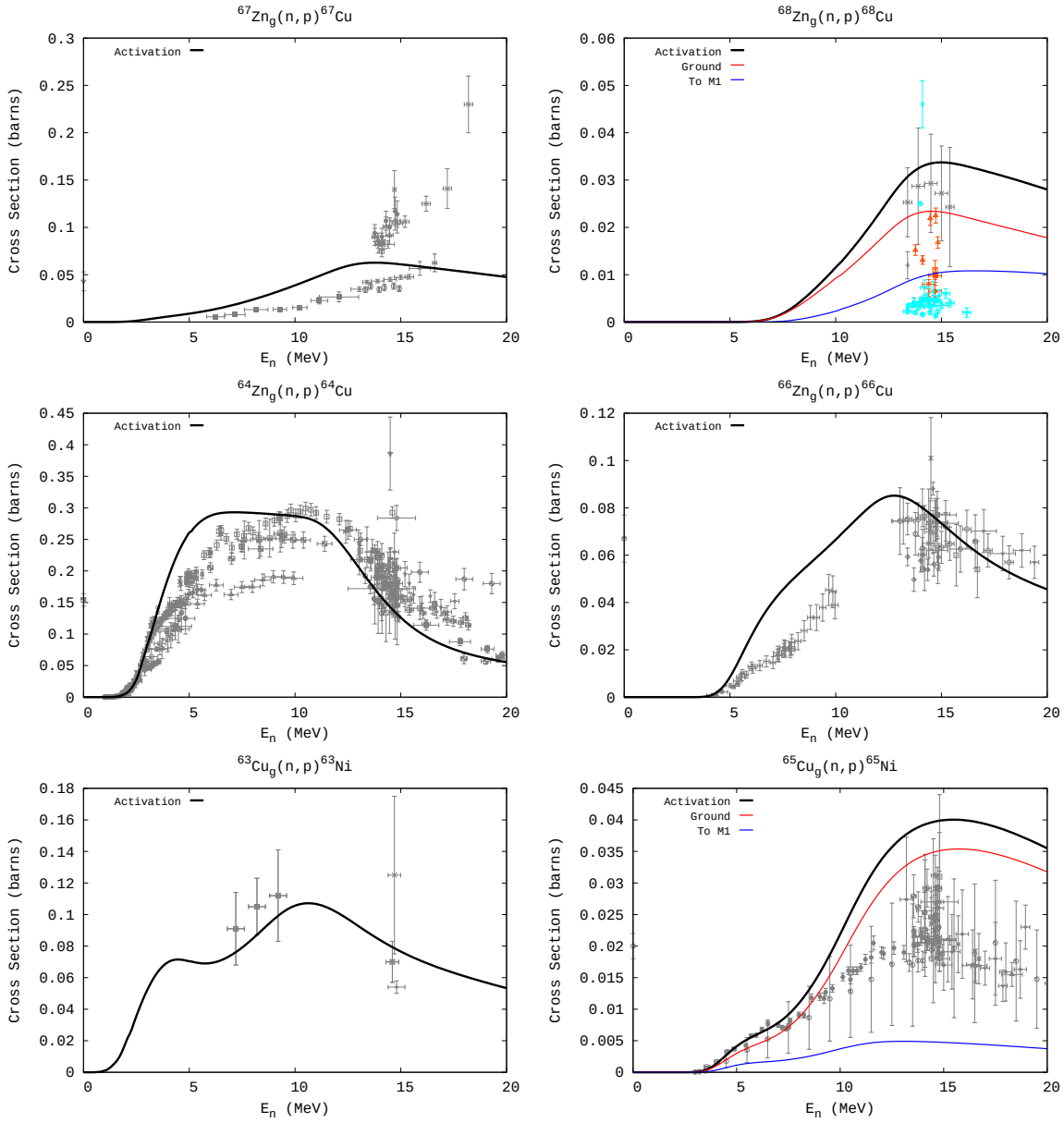

Fig. 6.— Calculated vs. measured (n,p) cross sections on select stable targets of Ni, Cu, and Zn. Measured cross sections are obtained from (CSISRS 2003). The solid black lines and grey data represent activation cross sections. Solid red lines and orange data represent the cross section going to the ground state of the residual (equal to the activation cross section when the residual nucleus does not have an isomer). Blue lines and cyan data represent the cross section going to the first isomer.

the only significant production channels leading to ^{64}Cu from loaded stable copper. The (n,3n) channel is also considered, but the threshold for this reaction is above 15 MeV and it will not be a factor in UGT analysis. We also consider possible neutron induced reactions leading to ^{64}Cu from zinc isotopes. However, since zinc is not a loaded isotope, production of copper through these channels should be relatively insignificant.

For the destruction reactions for ^{64}Cu, (n,p) dominates below ∼8 MeV, being roughly a factor of four larger than (n,γ) below 1 MeV. The (n,2n) reaction dominates above ∼8 MeV.

4. Conclusions

We have developed a new neutron threshold cross section set for radiochemical diagnos-

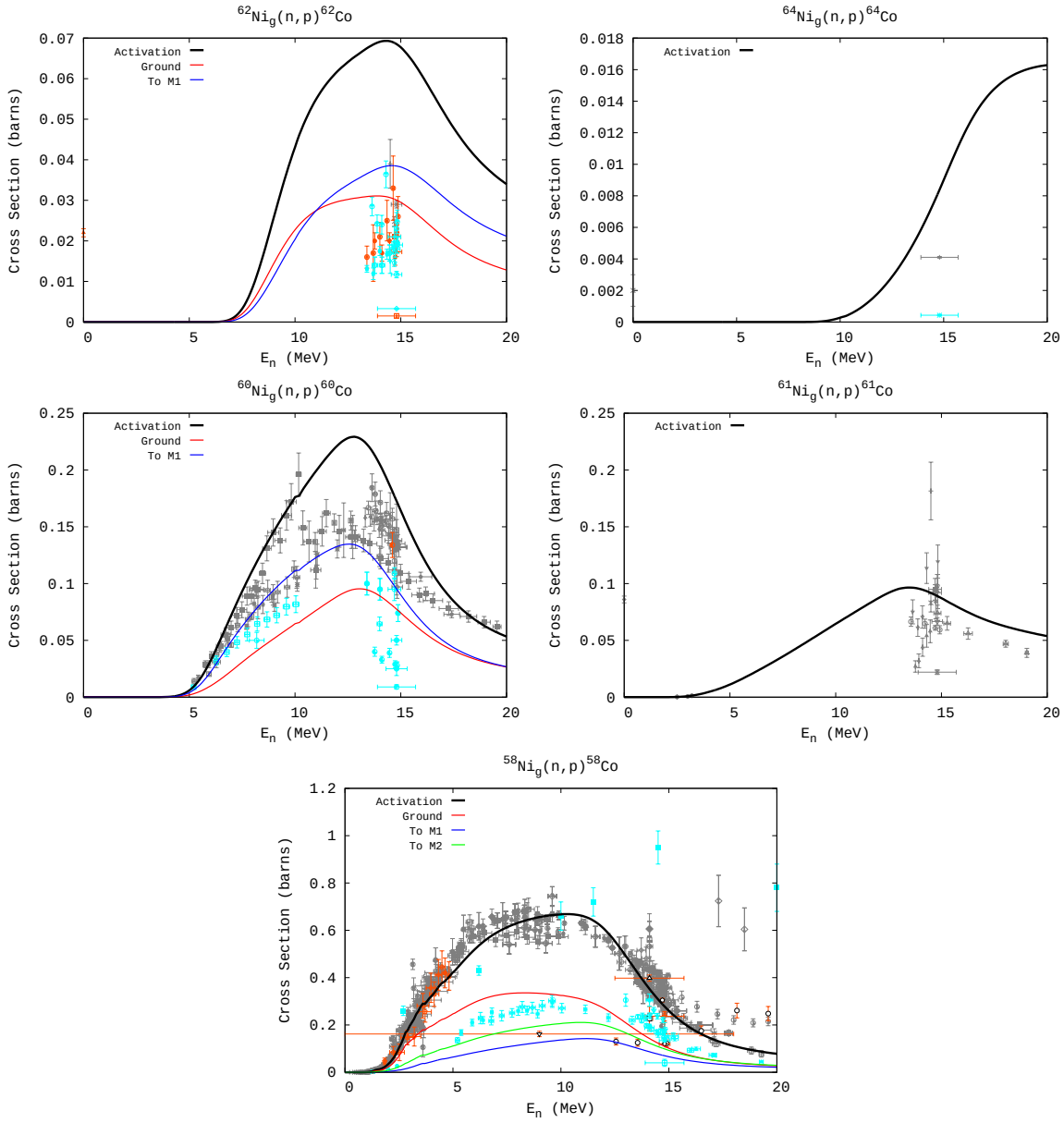

Fig. 6.— (continued)

tics of ^{64}Cu. The theory and implementation of the Hauser-Feshbach model were described, along with the details of the local systematics used to create a set of input parameters that reflect the latest available experimental data in the region of interest. The choice of our developed local systematics appears to do reasonably well in replicating measured cross sections in the region of interest.

Overall we consider the modeling effort to be quite successful, as our calculated cross sections do agree favorably with experimentally measured ones in this region of interest. Our calculations agree on average with measured (n,2n) cross sections to roughly 15%, which is generally representative of the spread in the existing experimental cross sections. Our neutron capture cross sections agree to roughly 40% (see Table 1). Lastly, our (n,p) cross sections are usually accurate to ∼30%. We identified these channels among the larger that can produce and destroy ^{64}Cu.

5. Acknowledgments

This work was performed under the auspices of the U.S. Department of Energy by the University

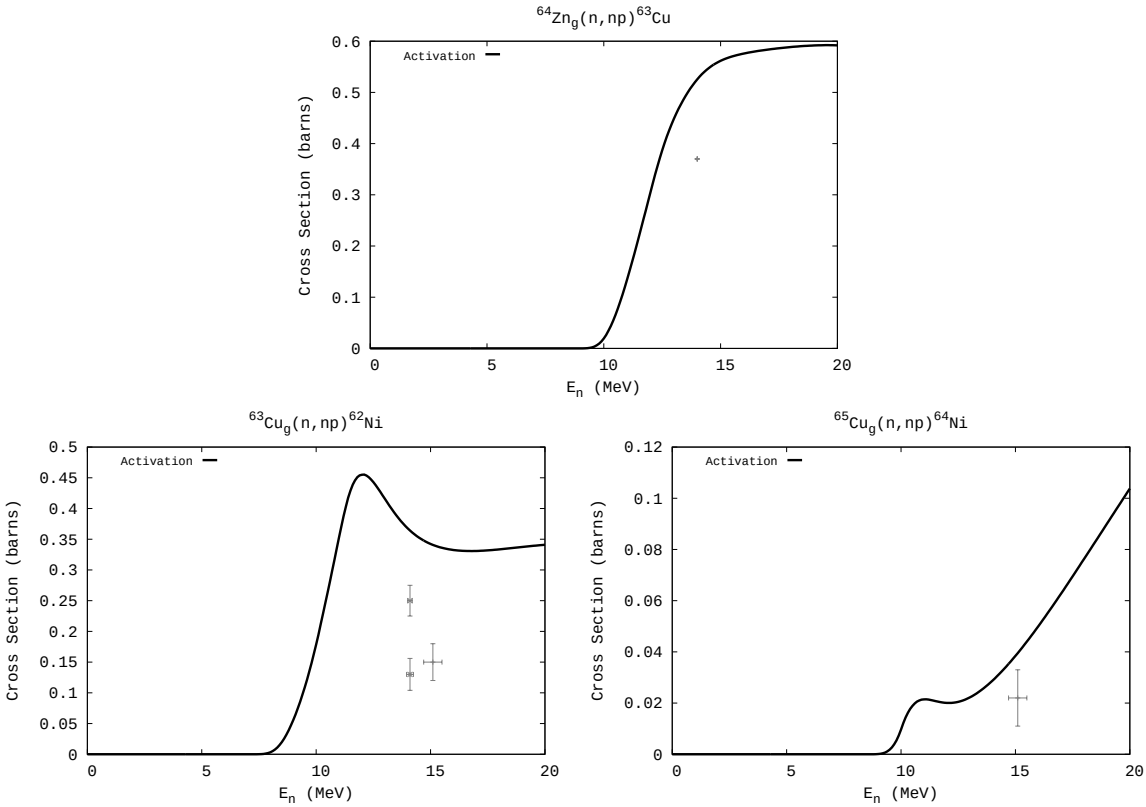

Fig. 7.— Calculated vs. measured (n,np)+(n,pn) cross sections on select stable targets of Ni, Cu, and Zn. Measured cross sections are obtained from (CSISRS 2003). The solid black lines and grey data represent activation cross sections. Solid red lines and orange data represent the cross section going to the ground state of the residual (equal to the activation cross section when the residual nucleus does not have an isomer). Blue lines and cyan data represent the cross section going to the first isomer.

of California Lawrence Livermore National Laboratory under contract W-7405-ENG-48.

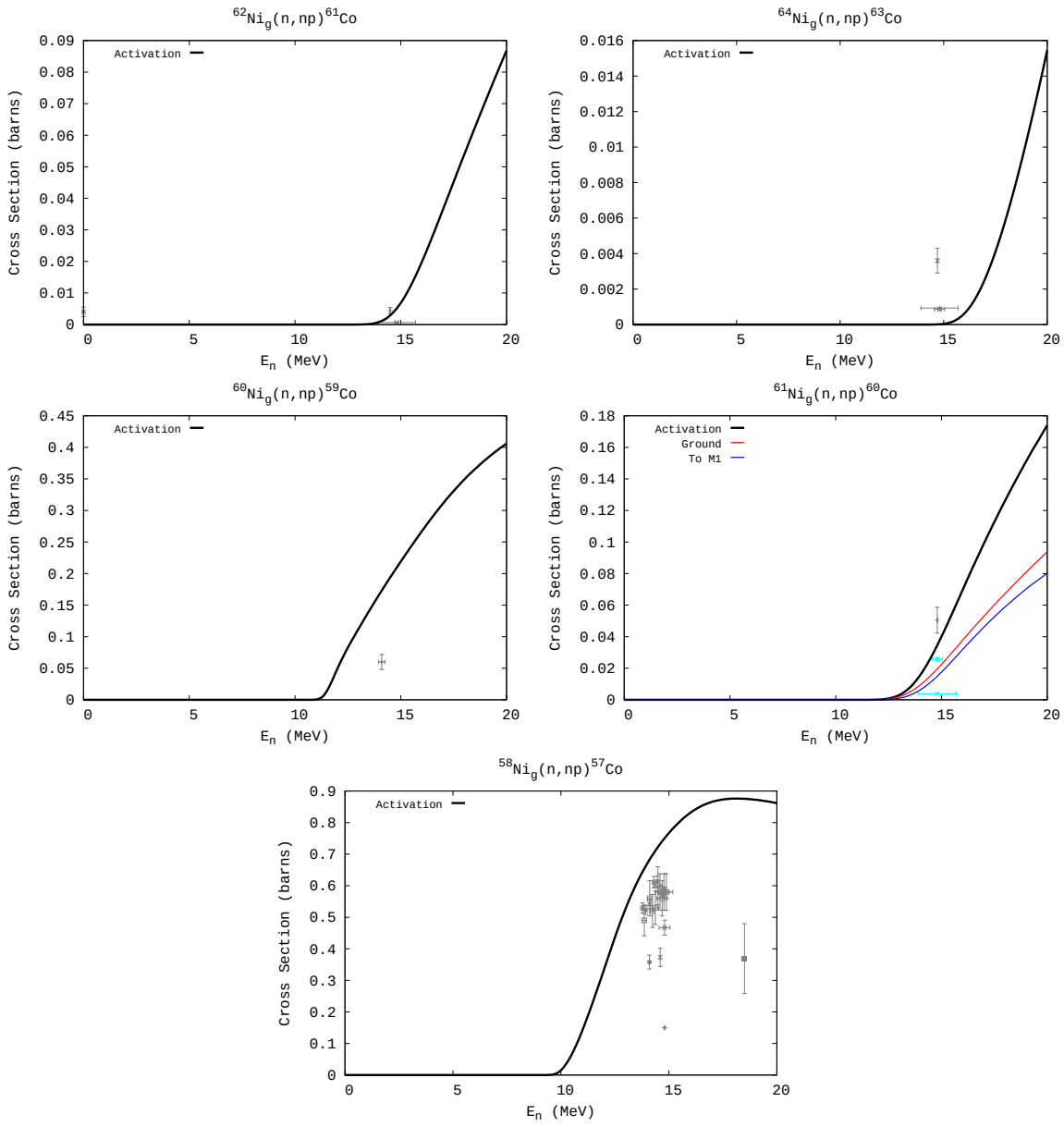

Fig. 7.— (continued)

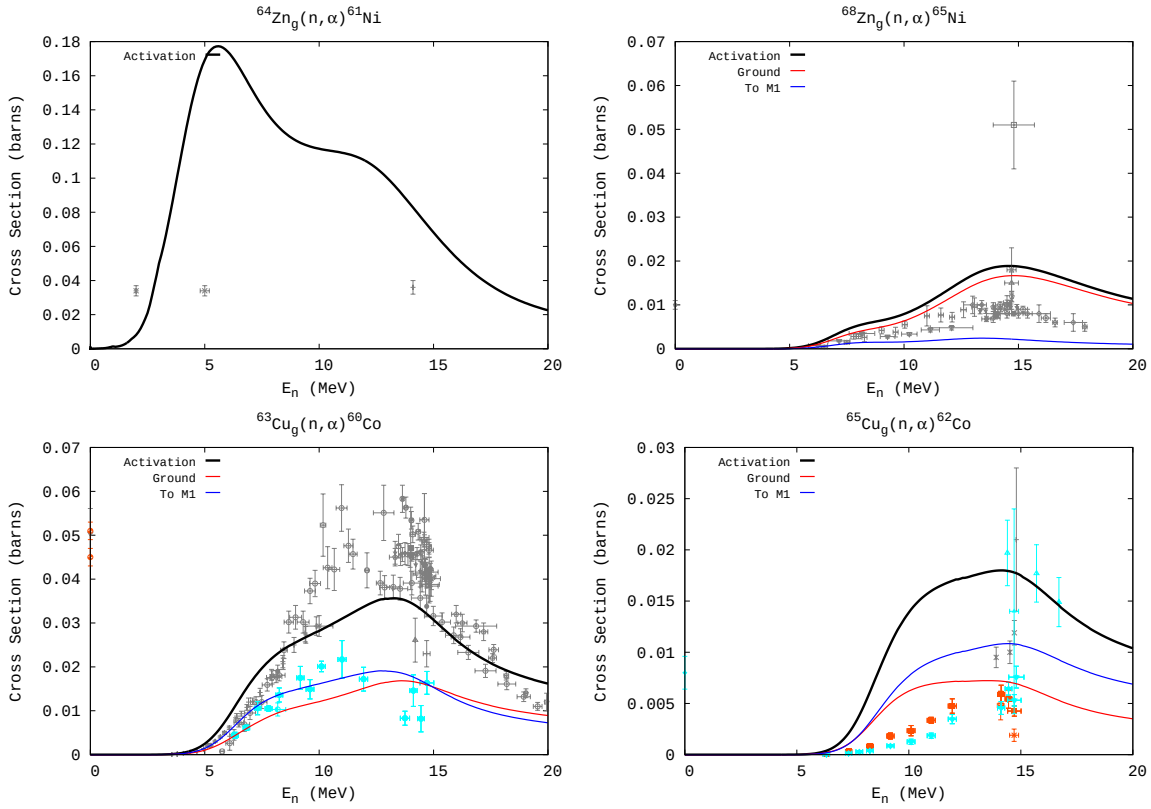

Fig. 8.— Calculated vs. measured (n,α) cross sections on select stable targets of Ni, Cu, and Zn. Measured cross sections are obtained from (CSISRS 2003). The solid black lines and grey data represent activation cross sections. Solid red lines and orange data represent the cross section going to the ground state of the residual (equal to the activation cross section when the residual nucleus does not have an isomer). Blue lines and cyan data represent the cross section going to the first isomer.

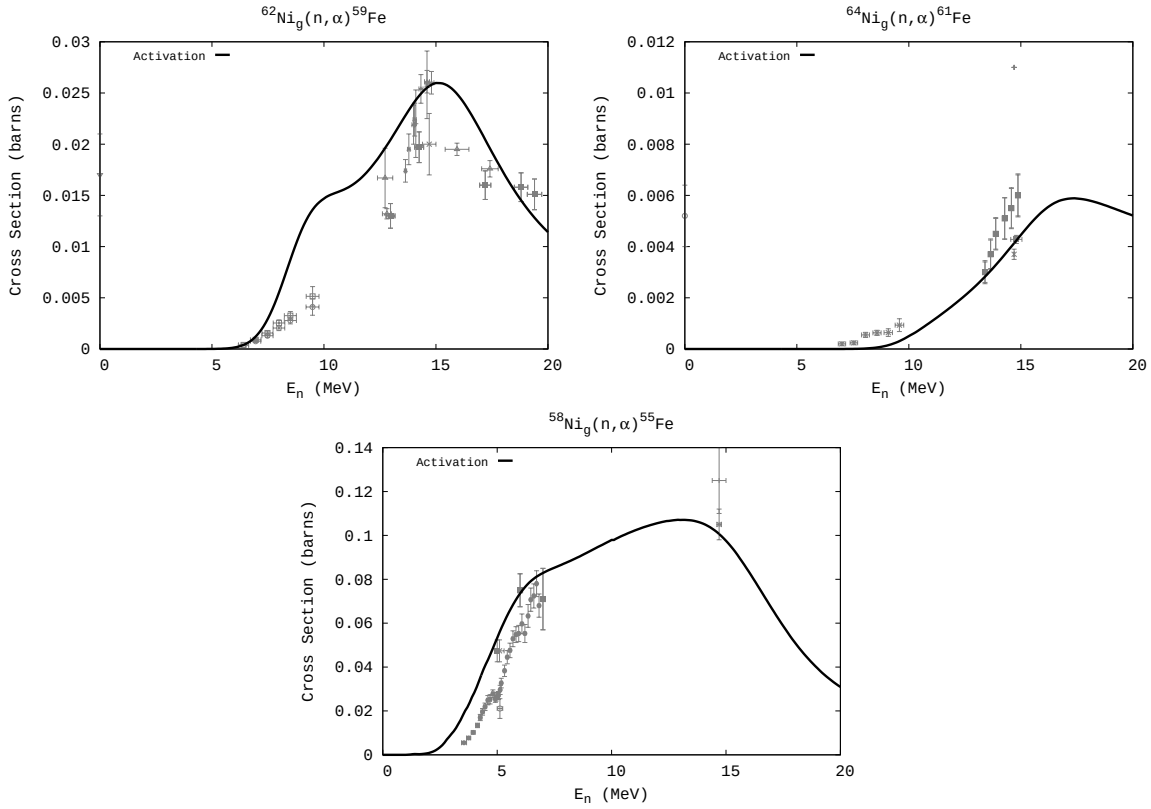

Fig. 8.— (continued)

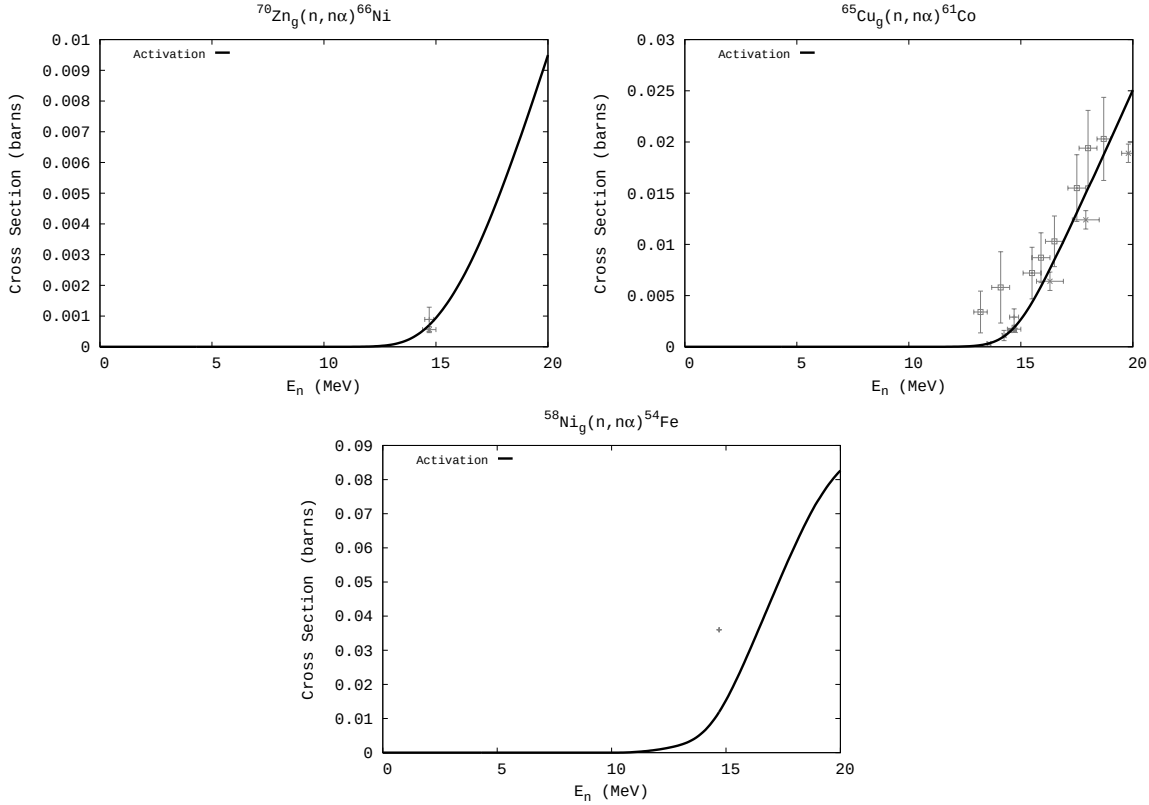

Fig. 9.— Calculated vs. measured (n,nα)+(n,αn) cross sections on select stable targets of Ni, Cu, and Zn. Measured cross sections are obtained from (CSISRS 2003). The solid black lines and grey data represent activation cross sections. Solid red lines and orange data represent the cross section going to the ground state of the residual (equal to the activation cross section when the residual nucleus does not have an isomer). Blue lines and cyan data represent the cross section going to the first isomer.

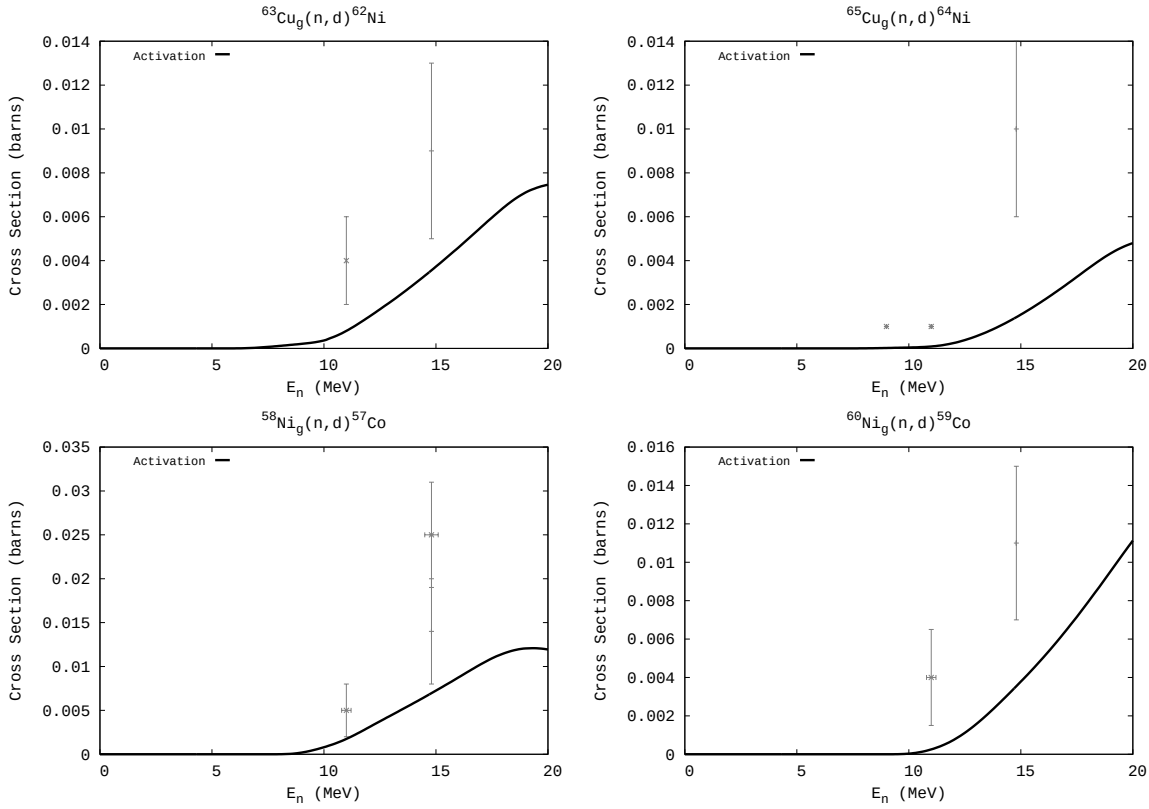

Fig. 10.— Calculated vs. measured (n,d) cross sections on select stable targets of Ni, Cu, and Zn. Measured cross sections are obtained from (CSISRS 2003). The solid black lines and grey data represent activation cross sections. Solid red lines and orange data represent the cross section going to the ground state of the residual (equal to the activation cross section when the residual nucleus does not have an isomer). Blue lines and cyan data represent the cross section going to the first isomer.

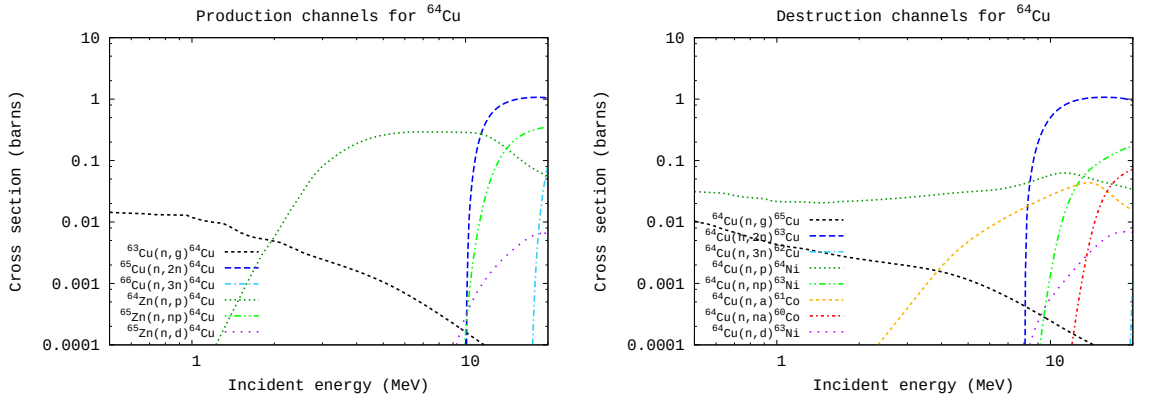

Fig. 11.— Calculated cross sections directly affecting production and destruction of ^{64}Cu.

REFERENCES

Avrigeanu, M. & Avrigeanu, V. IPNE-Bucharest Report No. NP-86-1995 (September 1995) http://www.nea.fr/abs/html/iaea0971.html

Avrigeanu, V., Hodgson, P.E., & Avrigeanu, M. 1994, Phys. Rev. **C49**, 2136

Bao, Z. Y., Beer, H., Kappeler, F.,, Voss, F., & Wisshak, K., 2000, Atomic Data & Nuclear Data Tables, **76**, 70

Beer, H., Voss, F., & Winters, R. R., 1992, ApJS, **80**, 403

Belgya, T., Bersillon, O., Copote Noy, R., Fukahori, T., Zhigang, G., Goriely, S., Herman, M., Ignatyuk, A.V., Kailas, S., Koning, A.J., Oblozinsky, P., Plujko, V, and Young, P.G., "Handbook for calculations of nuclear reaction data, RIPL-2", IAEA, Vienna (2005).

CSISRS: Experimental Nuclear Reaction Data File, Brookhaven National Laboratory, US Dept. of Energy, 2003. http://www.nndc.bnl.gov/nndc/exfor/

Cline, C. K., 1972, Nucl. Phys. **A195**, 353

ENSDF: Evaluated Nuclear Structure Data File, Brookhaven National Laboratory, US Dept. of Energy, http://www.nndc.bnl.gov/nndc/ensdf/

Gilbert, A., & Cameron, A.G.W., 1965, Can. J. Phys., **43**, 1446

Hoffman, R. D., Rauscher, T., Woosley, S. E. & Thielemann, F.-K., 1999, ApJ, **521**, 735

Hoffman, R.D., Dietrich, F.S., Bauer, R., Kelley, K., and Mustafa, M., 2004a, UCRL-TR-205563 (Br-Kr)

Hoffman, R.D., Dietrich, F.S., Bauer, R., Kelley, K., and Mustafa, M., 2004b, UCRL-TR-206721 (I-Xe)

Hoffman, R.D., Dietrich, F.S., Bauer, R., Kelley, K., and Mustafa, M., 2004c, UCRL-TR-211558 (Sm-Eu-Gd)

Kelley, K., Hoffman, R.D., Dietrich, F.S., Bauer, R., and Mustafa, M., 2005, UCRL-TR-211668 (Ti-V, Cr-Mn, Fe)

Kelley, K., Hoffman, R.D., Dietrich, F.S., and Mustafa, M., 2006, UCRL-TR-218181 (As)

Iljinov, A.S., Mebel, M.V., Bianchi, N., De Sanctis, E., Guaraldo, C., Lucherini, V., Muccifora, V., Polli, E., Reolon, A.R., & Rossi, P. 1992, Nucl. Phys. **A543**, 517

Koning, A.J., & Delaroche, J.P., 2003, Nucl. Phys. **A713**, 231

Lohr, J.M. & Haeberli, W. 1974, Nuc. Phys. **A232**, 381

Milazzo-Colli, L., and Braga-Marcazzan, G.M., 1973, Nuc. Phys. **A210**, 297

Möller, P., Nix, J.R., Myers, W.D., & Swiatecki, W.J., 1995, Atomic Data & Nuclear Data Tables, **59**, 185

Nethaway, D.R., Memo, "The Cross-Section Sets Used With the Watusi Program." LLNL A-Division memo, 5 Nov., 1998

Rauscher, T., Thielemann, F.-K., & Kratz, K.-L. 1997, Phys. Rev. C., **56**, 1613

Raynal, J. "ECIS96", Proceedings of the Specialists' Meeting on the Nucleon Nucleus Optical Model up to 200 MeV, 13-15 November 1996, Bruyeres-le-Chatel, Franc (http://www.nea.fr/html/science/om200/raynal.pdf)

Uhl, M., & Strohmaier, B. IRK-Vienna Report IRK-76/01 1976 (Upd. 1978)

Wapstra, A.H., Audi, G., & Thibault, C., 2003, Nuc. Phys. **A729**, 129

Williams, F. C. Jr., 1970, Phys. Lett. **31B**, 184

This 2-column preprint was prepared with the AAS LaTeX macros v5.0.

A. Basic Nuclear Structure Data

A.1. Adopted Spins, Parities, Binding Energies, and Separation Energies

This table lists the spin and parity assignments adopted for the ground states and isomers of each nucleus considered in this study. Also included are the binding energies and separation energies for neutrons, protons, alpha particles, and deuterons. For isomers, the energy of the isomer (given in parenthesis) should be subtracted from the binding and separation energies for the ground state.

Table 2:: Spins, parities, binding energies, and separation energies

^{A}Z	J^{π}	BE (MeV)	S_n (MeV)	S_p(MeV)	S_α (MeV)	S_d (MeV)
^{50}Cr	0+	435.049	13.000	9.591	8.561	18.920
^{51}Cr	7/2-	444.310	9.261	9.516	8.941	16.628
^{52}Cr	0+	456.349	12.039	10.505	9.354	19.331
^{53}Cr	3/2-	464.288	7.939	11.132	9.151	16.219
^{54}Cr	0+	474.007	9.719	12.373	7.931	18.627
^{55}Cr	3/2-	480.254	6.246	12.505	7.805	16.394
^{56}Cr	0+	488.499	8.245	13.419	8.241	18.526
^{57}Cr	3/2-	493.813	5.314	13.733	8.120	16.508
^{58}Cr	0+	501.195	7.382	14.935	8.665	18.890
^{59}Cr	3/2	505.323	4.128	14.972	8.646	16.839
^{60}Cr	0+	512.007	6.684	16.726	9.992	19.431
^{61}Cr	3/2	515.755	3.748	16.892	11.062	18.250
^{50}Mn	0+	426.634	13.083	4.585	7.979	12.943
^{50m}Mn	5+	(0.229)				
^{51}Mn	5/2-	440.320	13.686	5.271	8.664	16.047
^{52}Mn	6+	450.855	10.535	6.546	8.655	13.582
^{52m}Mn	2+	(0.378)				
^{53}Mn	7/2-	462.909	12.054	6.560	9.156	16.375
^{54}Mn	3+	471.848	8.939	7.560	8.759	13.274
^{55}Mn	5/2-	482.074	10.227	8.067	7.934	15.562
^{56}Mn	3+	489.345	7.270	9.091	7.893	13.113
^{57}Mn	5/2-	497.993	8.648	9.495	8.063	15.515
^{58}Mn	3+	504.485	6.491	10.672	8.441	13.761
^{58m}Mn	4+	(0.072)				
^{59}Mn	3/2-	512.129	7.644	10.934	8.753	16.091
^{60}Mn	3+	517.898	5.770	12.575	9.523	14.479
^{60m}Mn	3+	(0.272)				
^{61}Mn	5/2-	524.347	6.449	12.341	9.792	16.800
^{62}Mn	3+	528.902	4.554	13.147	10.255	14.671
^{63}Mn	5/2	535.285	6.384	13.226	11.710	17.306
^{64}Mn	1	539.622	4.337	14.379	12.464	15.338
^{51}Fe	5/2-	431.519	13.818	4.885	8.089	15.742
^{52}Fe	0+	447.699	16.181	7.379	7.937	18.840
^{53}Fe	7/2-	458.384	10.685	7.529	8.040	15.840
^{54}Fe	0+	471.763	13.378	8.854	8.418	18.683
^{55}Fe	3/2-	481.061	9.298	9.213	8.455	15.927
^{56}Fe	0+	492.258	11.197	10.184	7.613	18.186
^{57}Fe	1/2-	499.904	7.646	10.559	7.320	15.605
^{58}Fe	0+	509.949	10.045	11.956	7.646	18.379
^{59}Fe	3/2-	516.530	6.581	12.045	7.981	16.312
^{60}Fe	0+	525.350	8.820	13.221	8.555	18.641
^{61}Fe	3/2-	530.931	5.581	13.033	8.822	16.578
^{62}Fe	0+	538.981	8.051	14.634	9.491	18.859

Table 2: (continued)

^{A}Z	J^{π}	BE (MeV)	S_n (MeV)	S_p(MeV)	S_α (MeV)	S_d (MeV)
^{63}Fe	5/2-	543.698	4.716	14.796	10.079	17.126
^{64}Fe	0+	550.994	7.296	15.709	10.692	19.868
^{65}Fe	1/2	555.173	4.178	15.550	11.122	17.662
^{66}Fe	0+	561.939	6.767	16.190	11.584	20.092
^{67}Fe	1/2	566.130	4.190	16.727	12.590	18.155
^{52}Co	1	432.501	14.713	0.983	7.017	12.576
^{53}Co	7/2-	449.301	16.800	1.602	7.454	15.558
^{53m}Co	19/2-	(3.190)				
^{54}Co	0+	462.737	13.436	4.353	7.808	12.814
^{54m}Co	7+	(0.199)				
^{55}Co	7/2-	476.827	14.089	5.064	8.211	16.218
^{56}Co	4+	486.910	10.083	5.849	7.759	12.923
^{57}Co	7/2-	498.286	11.376	6.028	7.081	15.000
^{58}Co	2+	506.859	8.573	6.955	6.715	12.376
^{58m1}Co	5+	(0.025)				
^{58m2}Co	4+	(0.053)				
^{59}Co	7/2-	517.313	10.454	7.364	6.943	15.184
^{60}Co	5+	524.805	7.492	8.275	7.164	12.631
^{60m}Co	2+	(0.059)				
^{61}Co	7/2-	534.125	9.321	8.776	7.837	15.371
^{62}Co	2+	540.730	6.604	9.799	7.950	13.155
^{62m}Co	5+	(0.022)				
^{63}Co	7/2-	549.210	8.480	10.229	8.786	16.055
^{64}Co	1+	555.234	6.024	11.536	9.040	14.028
^{65}Co	7/2-	562.682	7.449	11.688	10.039	16.760
^{66}Co	3+	567.695	5.013	12.522	10.497	14.476
^{67}Co	7/2-	574.716	7.021	12.776	11.135	17.319
^{68}Co	4	579.077	4.361	12.947	11.159	14.913
^{54}Ni	0+	453.156	17.912	3.855	7.160	18.430
^{55}Ni	7/2-	467.352	14.196	4.615	7.538	15.826
^{56}Ni	0+	483.992	16.639	7.165	7.997	19.030
^{57}Ni	3/2-	494.241	10.250	7.332	7.562	15.190
^{58}Ni	0+	506.458	12.217	8.173	6.400	17.324
^{59}Ni	3/2-	515.458	8.999	8.599	6.101	14.947
^{60}Ni	0+	526.845	11.388	9.533	6.292	17.762
^{61}Ni	3/2-	534.665	7.820	9.861	6.466	15.128
^{62}Ni	0+	545.262	10.597	11.137	7.018	18.233
^{63}Ni	1/2-	552.100	6.838	11.370	7.274	15.750
^{64}Ni	0+	561.758	9.658	12.548	8.112	18.803
^{65}Ni	5/2-	567.856	6.098	12.622	8.630	16.421
^{65m}Ni	1/2-	(0.063)				
^{66}Ni	0+	576.808	8.952	14.125	9.530	19.349
^{67}Ni	1/2-	582.615	5.808	14.920	10.622	17.708
^{68}Ni	0+	590.408	7.793	15.692	11.118	20.488
^{69}Ni	9/2	594.994	4.586	15.917	11.526	18.053
^{55}Cu	1/2	452.858	18.001	-0.298	6.775	15.390
^{56}Cu	3	467.907	15.048	0.554	7.110	12.526
^{57}Cu	3/2-	484.687	16.780	0.695	7.090	15.110
^{58}Cu	1+	497.110	12.424	2.869	6.077	10.894
^{59}Cu	3/2-	509.877	12.767	3.418	4.755	13.411
^{60}Cu	2+	519.935	10.058	4.477	4.730	11.252

Table 2: (continued)

^{A}Z	J^{π}	BE (MeV)	S_n (MeV)	S_p(MeV)	S_α (MeV)	S_d (MeV)
^{61}Cu	3/2-	531.646	11.711	4.801	5.064	13.964
^{62}Cu	1+	540.531	8.885	5.866	5.377	11.461
^{63}Cu	3/2-	551.385	10.853	6.122	5.776	14.494
^{64}Cu	1+	559.301	7.916	7.201	6.200	11.814
^{65}Cu	3/2-	569.211	9.911	7.453	6.790	14.887
^{66}Cu	1+	576.277	7.066	8.421	7.252	12.295
^{67}Cu	3/2-	585.409	9.132	8.601	7.903	15.328
^{68}Cu	1+	591.729	6.320	9.113	8.199	12.696
^{68m}Cu	6-	(0.722)				
^{69}Cu	3/2-	599.969	8.240	9.561	8.991	15.129
^{70}Cu	1+	605.280	5.311	10.287	9.290	12.648
^{57}Zn	7/2-	469.395	15.143	1.488	5.855	14.312
^{58}Zn	0+	486.964	17.569	2.277	5.512	16.832
^{59}Zn	3/2-	499.998	13.034	2.887	4.350	13.087
^{60}Zn	0+	514.996	14.999	5.119	2.709	15.661
^{61}Zn	3/2-	525.225	10.229	5.290	2.688	13.124
^{62}Zn	0+	538.123	12.897	6.477	3.369	15.963
^{63}Zn	3/2-	547.236	9.113	6.704	3.482	13.365
^{64}Zn	0+	559.097	11.862	7.713	3.956	16.342
^{65}Zn	5/2-	567.077	7.979	7.776	4.116	13.468
^{65m}Zn	1/2-	(0.054)				
^{66}Zn	0+	578.136	11.059	8.925	4.578	16.611
^{67}Zn	5/2-	585.188	7.052	8.911	4.793	13.753
^{67m}Zn	1/2-	(0.093)				
^{68}Zn	0+	595.386	10.198	9.977	5.333	16.885
^{69}Zn	1/2-	601.869	6.482	10.140	5.717	14.235
^{69m}Zn	9/2+	(0.439)				
^{70}Zn	0+	611.086	9.218	11.117	5.983	17.133
^{71}Zn	1/2-	616.920	5.834	11.640	6.009	14.726
^{71m}Zn	9/2+	(0.158)				
^{58}Ga	3	467.870	16.156	-1.525	4.717	11.394
^{59}Ga	1/2	486.076	18.206	-0.888	4.922	14.457
^{60}Ga	1	500.024	13.948	0.026	3.822	10.836
^{61}Ga	3/2-	515.188	15.164	0.192	2.206	12.966
^{62}Ga	0+	528.169	12.981	2.944	2.763	10.948
^{63}Ga	3/2-	540.787	12.618	2.665	2.615	13.337
^{64}Ga	0+	551.146	10.359	3.910	2.915	10.799
^{65}Ga	3/2-	563.040	11.894	3.942	3.098	13.580
^{66}Ga	0+	572.179	9.139	5.102	3.352	10.856
^{67}Ga	3/2-	583.405	11.227	5.269	3.725	14.104
^{68}Ga	1+	591.683	8.278	6.495	4.087	11.322
^{69}Ga	3/2-	601.996	10.313	6.609	4.489	14.583
^{70}Ga	1+	609.649	7.654	7.781	5.077	12.038
^{71}Ga	3/2-	618.951	9.302	7.865	5.246	14.858
^{72}Ga	3-	625.471	6.520	8.552	5.447	12.160
^{72m}Ga	0+	(0.120)				

A.2. Q-values for Select Reactions

In this table we present the Q-values for each of the reactions considered in this study. These values are calculated from the binding energies listed in the previous table. For isomer targets, the energy of the isomer (given in parenthesis) should be added to the Q-value for the reaction on the ground state.

Table 3:: Q-values for activation reactions studied, in MeV

Target	(n,γ)	(n,2n)	(n,3n)	(n,p)	(n,np)	(n,α)	(n,nα)	(n,d)
^{58}Ni	8.999	-12.217	-22.467	0.400	-8.173	2.898	-6.400	-5.948
^{59}Ni	11.388	-8.999	-21.216	1.855	-8.599	5.096	-6.101	-6.374
^{60}Ni	7.820	-11.388	-20.387	-2.041	-9.533	1.354	-6.292	-7.308
^{61}Ni	10.597	-7.820	-19.208	-0.540	-9.861	3.579	-6.466	-7.636
^{62}Ni	6.838	-10.597	-18.417	-4.532	-11.137	-0.437	-7.018	-8.912
^{63}Ni	9.658	-6.838	-17.434	-2.890	-11.370	1.546	-7.274	-9.145
^{64}Ni	6.098	-9.658	-16.496	-6.524	-12.548	-2.531	-8.112	-10.323
^{65}Ni	8.951	-6.098	-15.756	-5.174	-12.622	-0.579	-8.630	-10.398
^{65m}Ni	(0.063)							
^{66}Ni	5.808	-8.951	-15.050	-9.113	-14.125	-4.814	-9.530	-11.901
^{67}Ni	7.793	-5.808	-14.759	-7.899	-14.920	-3.326	-10.622	-12.696
^{68}Ni	4.586	-7.793	-13.600	-11.331	-15.692	-6.940	-11.118	-13.467
^{59}Cu	10.058	-12.766	-25.190	5.581	-3.418	5.329	-4.755	-1.194
^{60}Cu	11.711	-10.058	-22.825	6.910	-4.477	6.646	-4.730	-2.253
^{61}Cu	8.885	-11.711	-21.769	3.020	-4.800	3.509	-5.064	-2.576
^{62}Cu	10.853	-8.885	-20.596	4.731	-5.866	5.077	-5.377	-3.641
^{63}Cu	7.916	-10.853	-19.739	0.715	-6.122	1.716	-5.776	-3.898
^{64}Cu	9.911	-7.916	-18.769	2.457	-7.201	3.121	-6.200	-4.976
^{65}Cu	7.066	-9.911	-17.827	-1.355	-7.453	-0.186	-6.790	-5.229
^{66}Cu	9.132	-7.066	-16.977	0.530	-8.421	1.228	-7.252	-6.197
^{67}Cu	6.320	-9.132	-16.198	-2.794	-8.602	-1.880	-7.903	-6.377
^{68}Cu	8.240	-6.320	-15.451	-1.321	-9.113	-0.751	-8.199	-6.889
^{68m}Cu	(0.722)							
^{69}Cu	5.311	-8.240	-14.560	-4.975	-9.561	-3.978	-8.991	-7.337
^{60}Zn	10.229	-14.999	-28.033	4.939	-5.120	7.541	-2.709	-2.895
^{61}Zn	12.897	-10.229	-25.228	6.420	-5.290	9.529	-2.688	-3.066
^{62}Zn	9.113	-12.897	-23.126	2.409	-6.477	5.631	-3.369	-4.252
^{63}Zn	11.862	-9.113	-22.010	4.149	-6.704	7.905	-3.482	-4.480
^{64}Zn	7.979	-11.862	-20.975	0.203	-7.713	3.864	-3.956	-5.488
^{65}Zn	11.059	-7.979	-19.841	2.134	-7.776	6.481	-4.116	-5.552
^{65m}Zn	(0.054)							
^{66}Zn	7.052	-11.059	-19.039	-1.859	-8.925	2.259	-4.578	-6.700
^{67}Zn	10.198	-7.052	-18.112	0.221	-8.911	4.865	-4.793	-6.686
^{67m}Zn	(0.093)							
^{68}Zn	6.482	-10.198	-17.250	-3.658	-9.977	0.765	-5.333	-7.753
^{69}Zn	9.218	-6.482	-16.680	-1.900	-10.140	3.235	-5.717	-7.915
^{69m}Zn	(0.439)							
^{70}Zn	5.834	-9.218	-15.700	-5.806	-11.117	-0.176	-5.983	-8.893

A.3. Nuclear Level Density Parameters

The following table presents our adopted level density parameters, as discussed in section 2.3. For each of the nuclei considered in this study (listed in the first column), we give the asymptotic level density parameter (column 2), whether the level density parameter is derived from a measured resonanace spacing or systematics ('x' and 's', respectively, in column 3), the backshift (column 4), the shell correction (column 5), and the ratio of the nuclear moment of inertia to that of a rigid sphere of equal volume (column 6). These are the parameters related to the Fermi-gas portion of the level density. The constant temperature parameters are given in columns 9 and 10, and the matching energy and value of the spin cutoff parameter at the matching energy are given in columns 7 and 8. The last column indicates the number of excited states used in our calculations. Nuclei for which only a ground state was included are indicated by a zero in this column.

Table 4:: Adopted level density parameters

^{A}Z	$\tilde{a}(A)$ (MeV)$^{-1}$	x/s	Δ (MeV)	δW (MeV)	λ	E_x (MeV)	$\sigma^2(E_x)$	E_0 (MeV)	T (MeV)	N
^{50}Cr	5.644	s	2.015	1.76	1.003	6.372	2.932	-1.217	1.205	7
^{51}Cr	5.914	x	0.048	0.36	0.946	4.820	2.973	-3.386	1.241	12
^{52}Cr	5.917	s	2.011	0.12	1.003	8.881	3.417	-2.869	1.406	15
^{53}Cr	6.021	x	0.448	0.07	1.000	6.047	3.281	-3.529	1.298	13
^{54}Cr	6.030	x	1.945	0.74	0.912	7.603	3.166	-2.130	1.283	9
^{55}Cr	6.226	x	0.354	1.57	0.913	6.640	3.248	-4.257	1.282	7
^{56}Cr	6.465	s	1.714	1.98	0.912	4.605	2.673	-0.495	0.965	7
^{57}Cr	6.602	s	0.248	2.67	0.914	5.380	3.099	-3.569	1.121	0
^{58}Cr	6.740	s	1.814	2.90	0.913	6.900	3.112	-1.980	1.097	0
^{59}Cr	6.878	s	-0.040	3.34	0.925	5.002	3.141	-3.825	1.069	0
^{60}Cr	7.017	s	1.830	3.25	0.919	6.830	3.155	-1.916	1.054	0
^{61}Cr	7.156	s	0.297	4.28	0.875	5.256	3.068	-3.471	1.016	0
^{50}Mn	5.644	s	-0.226	1.17	0.897	7.162	3.188	-5.621	1.460	1
^{51}Mn	5.780	s	0.261	0.37	0.909	5.651	3.022	-3.601	1.310	11
^{52}Mn	5.917	s	-0.625	0.02	0.927	1.589	2.478	-2.518	1.044	24
^{53}Mn	6.053	s	0.205	-0.27	1.000	6.278	3.357	-4.068	1.338	21
^{54}Mn	6.190	s	-0.735	-0.21	0.933	6.478	3.416	-5.820	1.397	17
^{55}Mn	6.327	s	0.210	0.68	0.906	4.956	3.032	-3.212	1.173	12
^{56}Mn	6.624	x	-0.712	1.50	0.903	7.832	3.492	-7.084	1.387	8
^{57}Mn	6.602	s	-0.076	1.96	0.905	3.428	2.821	-2.682	1.004	6
^{58}Mn	6.740	s	-0.632	2.56	0.905	6.806	3.424	-6.267	1.277	1
^{59}Mn	6.878	s	-0.103	2.80	0.912	4.939	3.136	-3.857	1.081	0
^{60}Mn	7.017	s	-0.284	3.16	0.910	3.042	2.834	-2.776	0.918	1
^{61}Mn	7.156	s	-0.100	3.34	0.905	4.859	3.149	-3.819	1.035	0
^{62}Mn	7.294	s	-0.870	3.96	0.884	4.049	3.115	-4.590	1.006	0
^{63}Mn	7.434	s	-0.109	3.71	0.883	4.772	3.141	-3.785	0.996	0
^{64}Mn	7.573	s	-0.741	4.02	0.880	4.103	3.147	-4.404	0.975	0
^{51}Fe	5.780	s	0.385	0.64	0.909	4.565	2.826	-2.675	1.204	0
^{52}Fe	5.917	s	2.818	0.53	1.000	6.873	2.976	-0.147	1.177	5
^{53}Fe	6.053	s	0.121	-0.73	0.948	4.999	3.111	-3.309	1.262	5
^{54}Fe	6.190	s	1.967	-1.01	1.000	8.249	3.448	-2.367	1.354	25
^{55}Fe	6.359	x	0.366	-0.97	1.000	4.783	3.185	-2.741	1.192	5
^{56}Fe	6.465	s	1.927	0.05	1.002	9.182	3.605	-3.231	1.355	33
^{57}Fe	6.420	x	0.302	0.72	0.911	7.283	3.436	-4.741	1.326	31
^{58}Fe	6.527	x	2.014	1.22	0.914	9.433	3.513	-3.428	1.331	32
^{59}Fe	6.910	x	0.383	1.94	0.915	4.950	3.087	-2.968	1.060	28
^{60}Fe	7.017	s	1.921	2.07	0.918	6.898	3.188	-1.740	1.078	24
^{61}Fe	7.156	s	0.191	2.38	0.910	4.974	3.160	-3.340	1.042	4

Table 4: (continued)

^{A}Z	$\tilde{a}(A)$ $(\mathrm{MeV})^{-1}$	x/s	Δ (MeV)	δW (MeV)	λ	E_x (MeV)	$\sigma^2(E_x)$	E_0 (MeV)	T (MeV)	N
^{62}Fe	7.294	s	1.935	2.59	0.922	6.471	3.159	-1.420	1.005	4
^{63}Fe	7.434	s	0.170	3.10	1.098	5.051	3.524	-3.474	1.008	0
^{64}Fe	7.573	s	1.785	2.70	1.065	6.629	3.507	-1.809	1.002	0
^{65}Fe	7.713	s	0.110	2.60	1.022	4.918	3.462	-3.451	0.989	0
^{66}Fe	7.852	s	1.498	2.24	0.988	6.271	3.438	-2.016	0.982	0
^{67}Fe	7.992	s	0.616	2.81	0.972	5.355	3.412	-2.903	0.957	0
^{52}Co	5.917	s	-0.962	0.12	0.933	4.423	3.101	-4.797	1.296	0
^{53}Co	6.053	s	0.278	-0.86	0.948	1.336	2.129	-1.483	1.082	1
^{54}Co	6.190	s	-0.229	-1.17	0.953	3.462	2.955	-2.890	1.164	2
^{55}Co	6.327	s	0.476	-2.18	0.977	4.041	3.035	-2.070	1.171	9
^{56}Co	6.465	s	-0.694	-1.54	0.949	3.771	3.167	-3.794	1.200	7
^{57}Co	6.602	s	0.165	-0.89	0.948	4.757	3.193	-3.052	1.172	7
^{58}Co	6.740	s	-0.881	0.11	0.931	5.252	3.393	-5.236	1.241	11
^{59}Co	6.878	s	0.198	0.77	0.931	4.867	3.175	-3.164	1.100	31
^{60}Co	7.057	x	-0.854	1.39	0.921	4.209	3.225	-4.536	1.096	49
^{61}Co	7.156	s	0.089	1.75	0.927	1.248	2.248	-1.185	0.774	2
^{62}Co	7.294	s	-0.862	2.35	0.937	9.702	3.957	-9.109	1.411	1
^{63}Co	7.434	s	0.034	2.41	0.945	0.904	2.133	-1.153	0.733	1
^{64}Co	7.573	s	-0.628	2.89	0.954	2.734	3.021	-3.124	0.879	0
^{65}Co	7.713	s	-0.000	2.56	0.968	4.808	3.370	-3.558	0.990	0
^{66}Co	7.852	s	-1.102	2.59	0.974	3.671	3.401	-4.635	0.975	0
^{67}Co	7.992	s	-0.064	2.23	0.974	4.675	3.436	-3.552	0.969	0
^{68}Co	8.133	s	-1.333	2.45	0.972	3.373	3.446	-4.808	0.951	0
^{54}Ni	6.190	s	1.967	-1.14	1.000	7.245	3.307	-1.688	1.286	0
^{55}Ni	6.327	s	0.404	-2.17	0.979	3.276	2.879	-1.773	1.118	0
^{56}Ni	6.465	s	3.215	-2.74	1.003	8.057	3.373	-0.028	1.267	23
^{57}Ni	6.602	s	0.624	-2.67	1.014	2.378	2.662	-1.070	1.037	9
^{58}Ni	6.740	s	1.993	-1.58	1.003	9.978	3.833	-3.427	1.405	29
^{59}Ni	6.860	x	0.433	-0.68	1.003	7.384	3.702	-4.413	1.302	32
^{60}Ni	6.848	x	2.075	-0.16	0.989	10.154	3.850	-3.668	1.364	34
^{61}Ni	7.284	x	0.305	0.59	1.100	5.540	3.607	-3.446	1.105	28
^{62}Ni	7.110	x	2.193	1.10	1.068	9.757	3.954	-3.362	1.273	37
^{63}Ni	7.644	x	0.337	1.58	1.098	2.995	3.051	-1.657	0.843	22
^{64}Ni	7.573	s	2.164	1.63	1.067	6.755	3.502	-1.181	1.006	23
^{65}Ni	8.032	x	0.337	1.76	1.057	2.519	2.882	-1.342	0.767	22
^{66}Ni	7.852	s	2.167	1.55	0.989	4.868	3.003	0.154	0.831	2
^{67}Ni	7.992	s	0.956	1.25	1.014	4.872	3.377	-1.879	0.927	1
^{68}Ni	8.133	s	2.334	1.02	0.992	6.711	3.471	-0.821	0.957	2
^{69}Ni	8.273	s	0.744	1.69	1.035	5.418	3.606	-2.665	0.954	0
^{55}Cu	6.327	s	0.316	-0.63	0.946	5.543	3.221	-3.344	1.248	0
^{56}Cu	6.465	s	-0.666	-0.94	0.942	4.513	3.250	-4.267	1.235	0
^{57}Cu	6.602	s	0.693	-2.31	1.029	2.963	2.844	-1.170	1.045	0
^{58}Cu	6.740	s	-0.090	-1.21	0.948	3.765	3.097	-2.819	1.108	5
^{59}Cu	6.878	s	0.252	-0.65	0.935	2.214	2.605	-1.416	0.925	8
^{60}Cu	7.017	s	-0.616	0.35	0.918	6.769	3.585	-5.926	1.288	6
^{61}Cu	7.156	s	0.287	0.88	0.926	4.269	3.093	-2.595	1.014	31
^{62}Cu	7.294	s	-0.701	1.53	0.922	5.351	3.435	-5.139	1.142	18
^{63}Cu	7.434	s	0.337	1.86	0.925	2.621	2.706	-1.435	0.821	10
^{64}Cu	7.216	x	-0.643	2.42	0.928	3.940	3.277	-4.025	1.020	16
^{65}Cu	7.713	s	0.343	2.33	1.124	1.794	2.693	-0.950	0.718	14

Table 4: (continued)

^{A}Z	$\tilde{a}(A)$ $(\mathrm{MeV})^{-1}$	x/s	Δ (MeV)	δW (MeV)	λ	E_x (MeV)	$\sigma^2(E_x)$	E_0 (MeV)	T (MeV)	N
^{66}Cu	7.706	x	-0.639	2.69	1.123	4.020	3.644	-4.090	0.977	6
^{67}Cu	7.992	s	0.359	2.36	1.089	1.438	2.500	-0.768	0.676	0
^{68}Cu	8.133	s	-0.737	2.62	0.968	0.000	2.153	-1.825	0.670	3
^{69}Cu	8.273	s	0.343	2.30	0.968	1.825	2.595	-0.923	0.679	0
^{70}Cu	8.414	s	-0.962	2.51	0.967	2.275	3.174	-3.343	0.814	0
^{57}Zn	6.602	s	0.147	-0.30	0.934	5.279	3.235	-3.470	1.196	0
^{58}Zn	6.740	s	1.925	-1.01	1.005	7.011	3.408	-1.605	1.196	0
^{59}Zn	6.878	s	0.224	-0.32	0.927	5.266	3.270	-3.327	1.157	0
^{60}Zn	7.017	s	2.424	0.35	0.911	7.325	3.223	-1.074	1.114	2
^{61}Zn	7.156	s	-0.081	1.16	0.908	4.596	3.180	-3.467	1.062	9
^{62}Zn	7.294	s	1.899	1.57	0.907	5.904	3.069	-1.023	0.986	3
^{63}Zn	7.434	s	0.011	2.26	0.908	4.659	3.192	-3.411	1.008	11
^{64}Zn	7.573	s	1.913	2.53	0.906	6.167	3.136	-1.225	0.959	10
^{65}Zn	7.729	x	-0.101	2.88	1.247	4.543	3.778	-3.550	0.970	8
^{66}Zn	7.852	s	1.916	2.89	1.185	6.343	3.670	-1.367	0.943	10
^{67}Zn	7.983	x	-0.182	3.16	1.151	3.969	3.578	-3.265	0.906	8
^{68}Zn	7.982	x	1.771	2.99	1.124	6.706	3.747	-1.910	0.969	31
^{69}Zn	8.329	x	-0.094	3.33	1.128	2.343	3.134	-1.930	0.735	4
^{70}Zn	8.414	s	1.659	2.94	0.975	6.517	3.516	-1.962	0.932	2
^{71}Zn	8.638	x	0.012	3.25	0.970	4.583	3.461	-3.400	0.890	2
^{58}Ga	6.740	s	-0.969	0.61	0.920	4.117	3.201	-4.618	1.152	0
^{59}Ga	6.878	s	0.609	-0.20	1.005	5.651	3.400	-2.950	1.154	0
^{60}Ga	7.017	s	-0.552	0.69	0.913	4.448	3.230	-4.142	1.113	0
^{61}Ga	7.156	s	-0.017	1.21	0.909	4.942	3.227	-3.611	1.083	0
^{62}Ga	7.294	s	0.277	1.94	0.904	5.196	3.214	-3.331	1.049	0
^{63}Ga	7.434	s	-0.042	2.30	0.905	4.839	3.225	-3.642	1.025	0
^{64}Ga	7.573	s	-0.624	2.76	0.909	5.347	3.415	-5.109	1.083	15
^{65}Ga	7.713	s	0.110	2.98	0.909	3.910	3.064	-2.705	0.902	6
^{66}Ga	7.852	s	-0.802	3.40	1.263	5.338	4.096	-5.482	1.058	37
^{67}Ga	7.992	s	0.207	3.69	0.912	3.160	2.906	-2.001	0.795	6
^{68}Ga	8.133	s	-0.711	3.89	1.196	3.656	3.696	-3.990	0.897	23
^{69}Ga	8.273	s	0.186	3.79	1.181	3.079	3.339	-1.974	0.769	5
^{70}Ga	8.328	x	-0.538	3.94	1.170	3.603	3.671	-3.640	0.865	26
^{71}Ga	8.555	s	0.228	3.71	1.166	4.756	3.777	-3.171	0.883	3
^{72}Ga	8.828	x	-1.027	3.92	1.175	4.550	4.005	-5.295	0.937	12

B. Modeled Cross Sections: Production and Destruction Channels

Here we present the activation cross sections for the various neutron induced reaction channels producing a given isotope and destroying the ground state of that isotope.

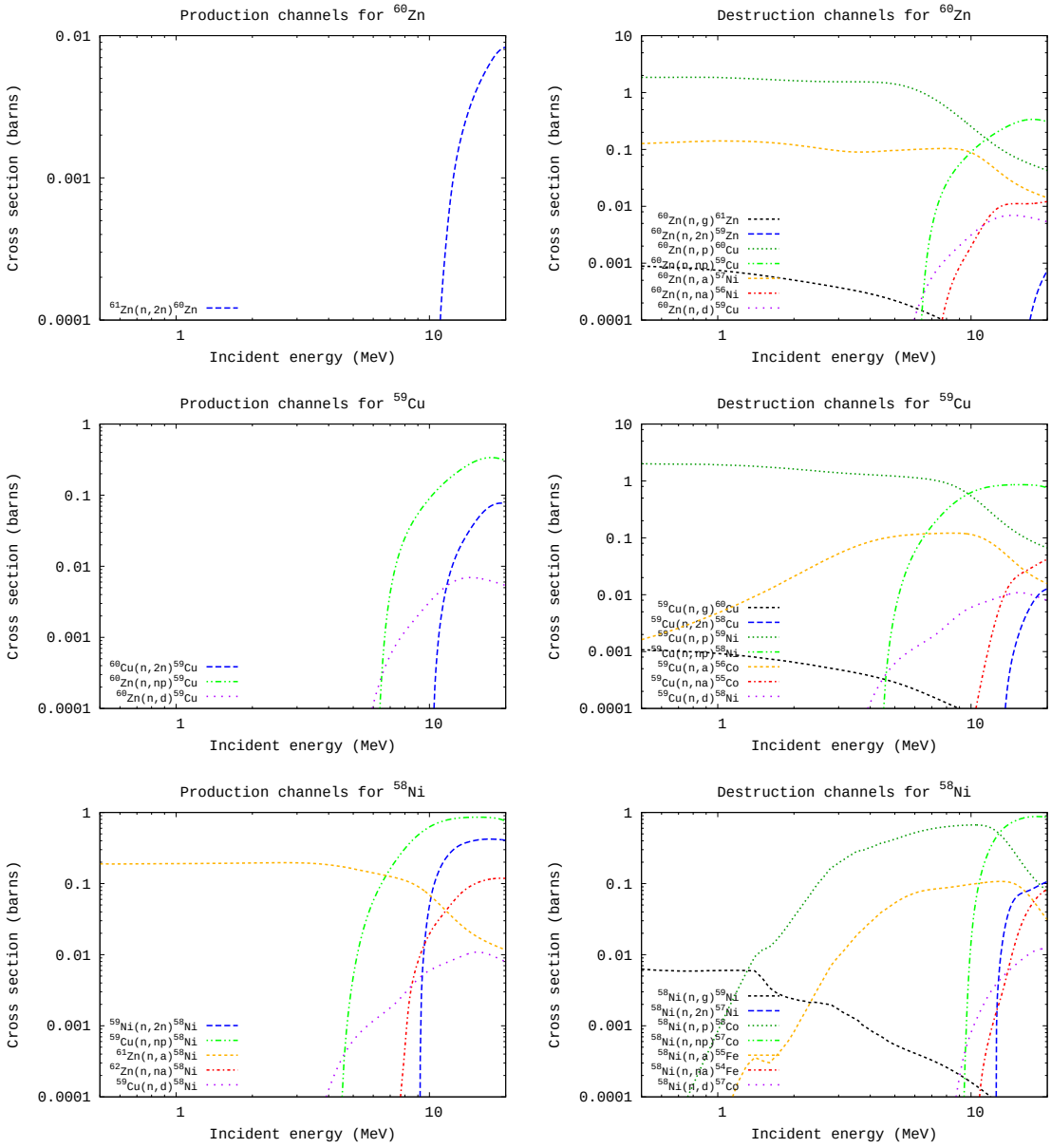

Fig. 12.— Production and destruction cross sections

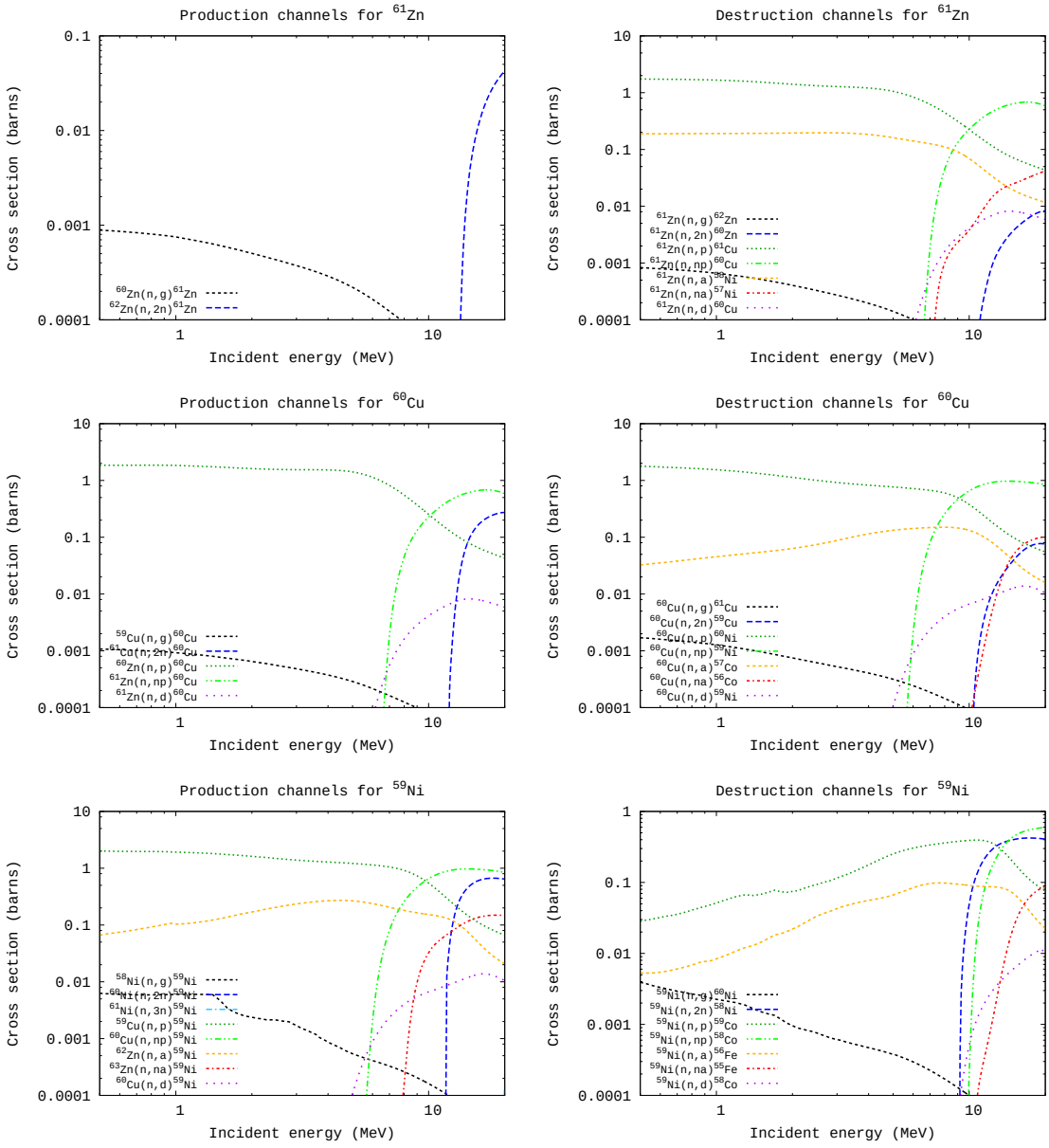

Fig. 12.— (continued)

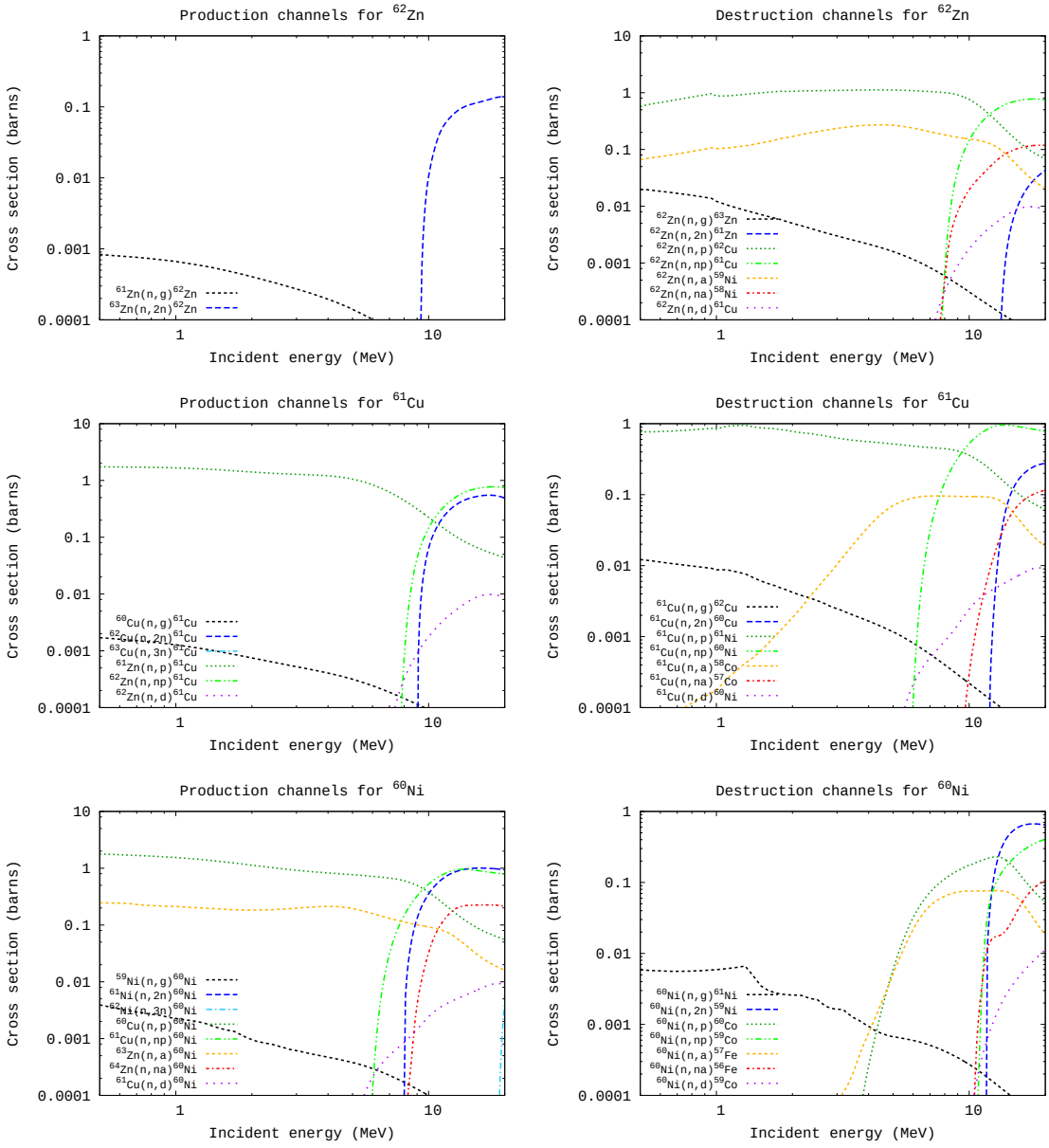

Fig. 12.— (continued)

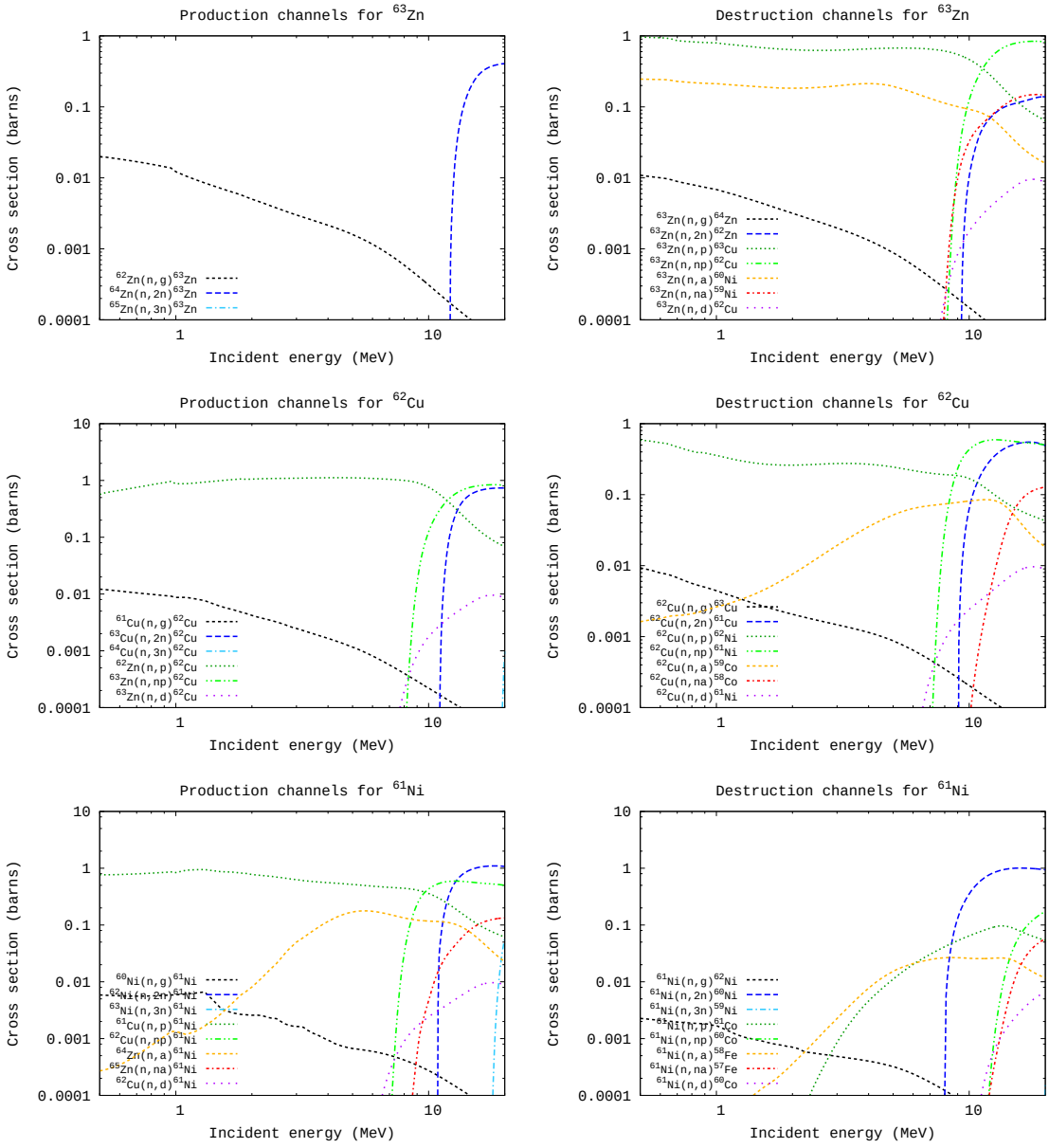

Fig. 12.— (continued)

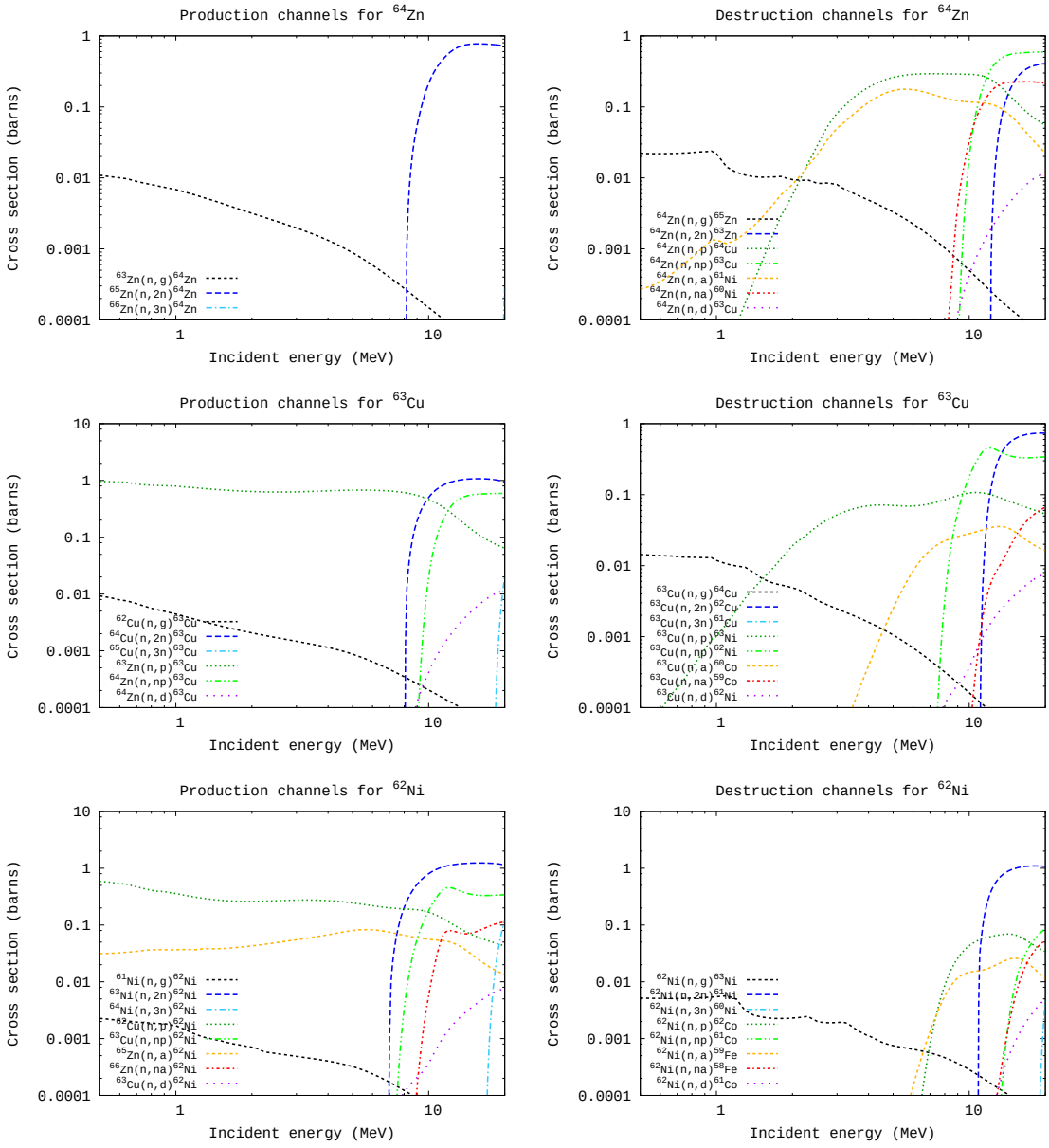

Fig. 12.— (continued)

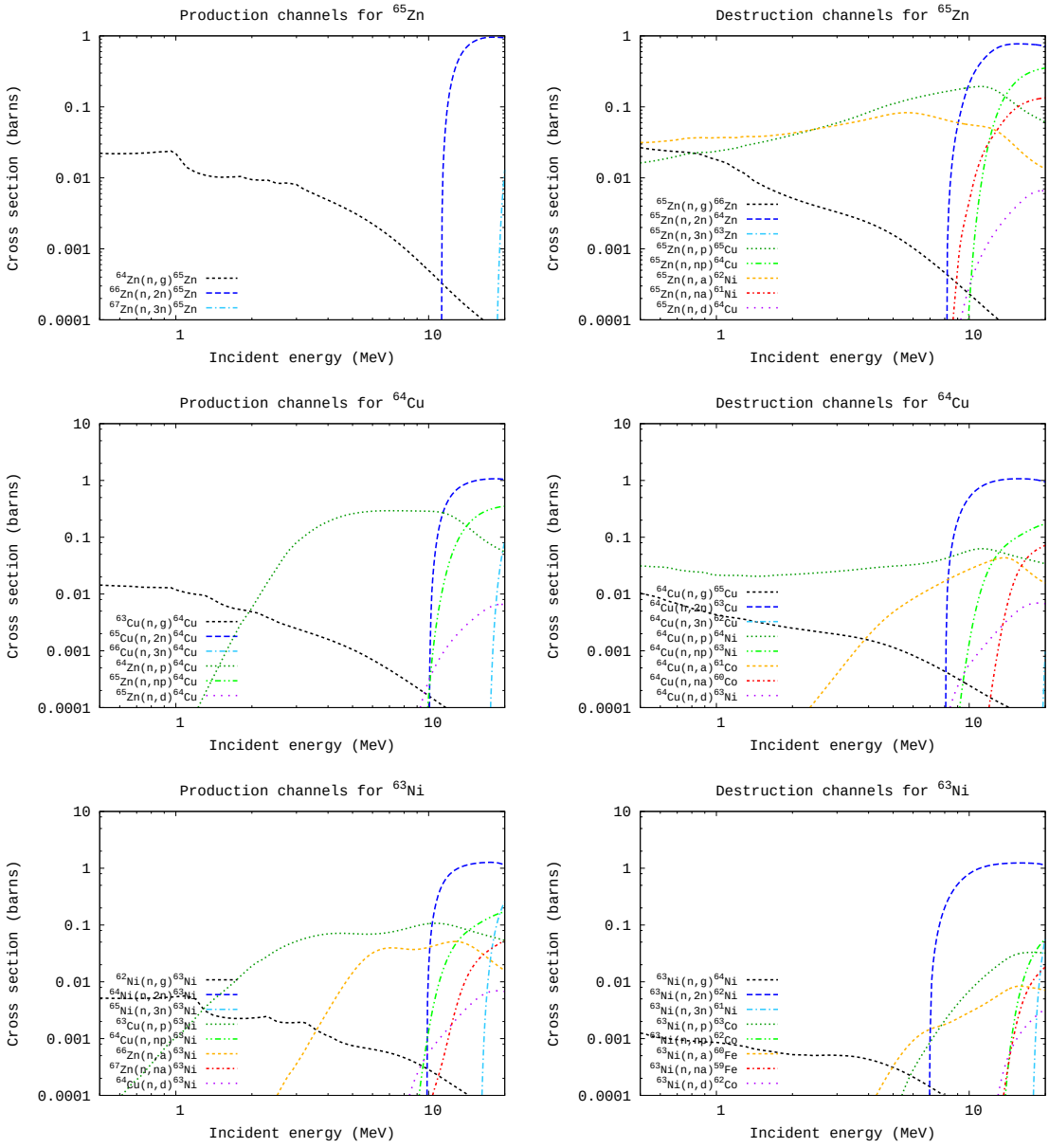

Fig. 12.— (continued)

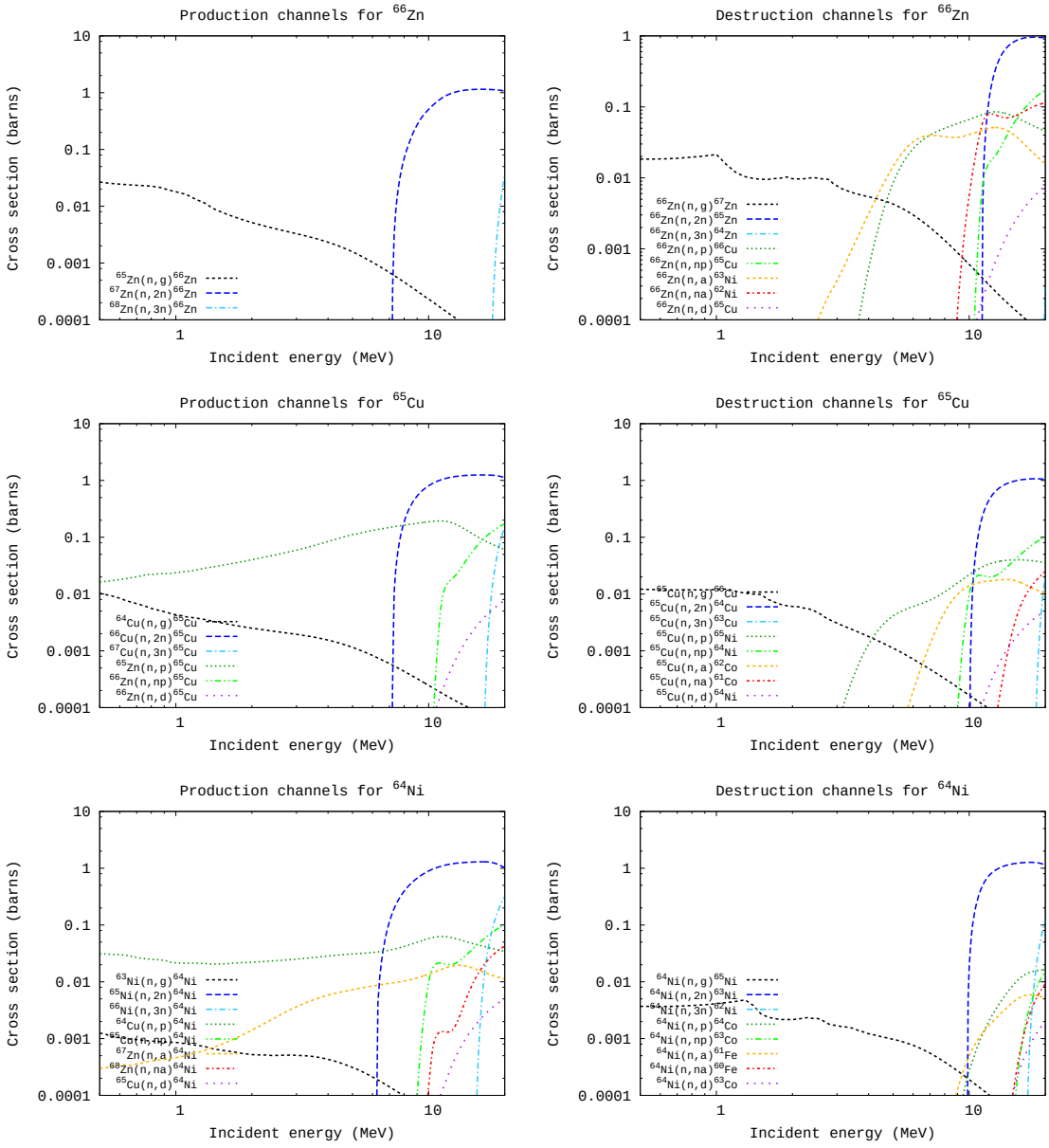

Fig. 12.— (continued)

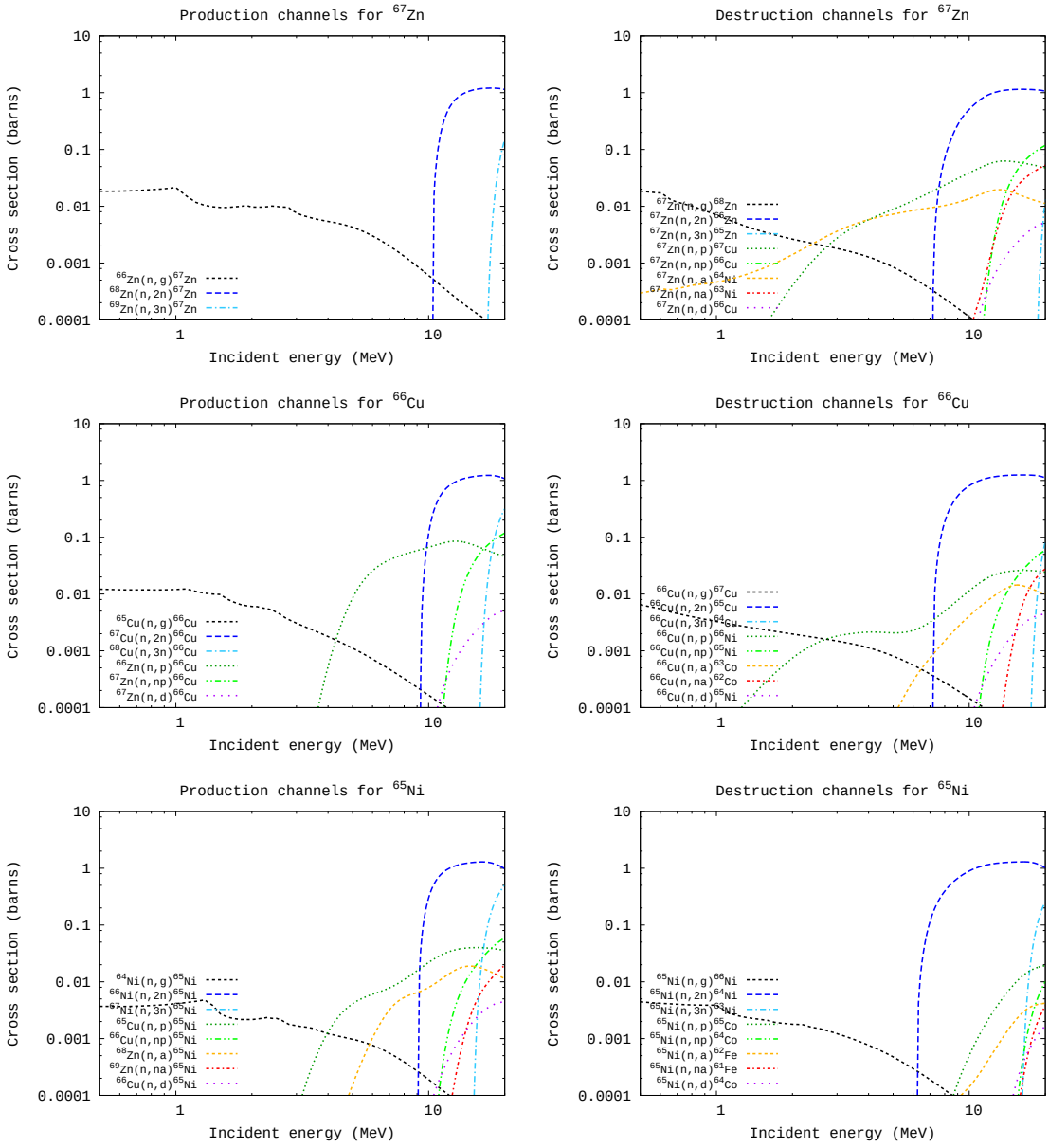

Fig. 12.— (continued)

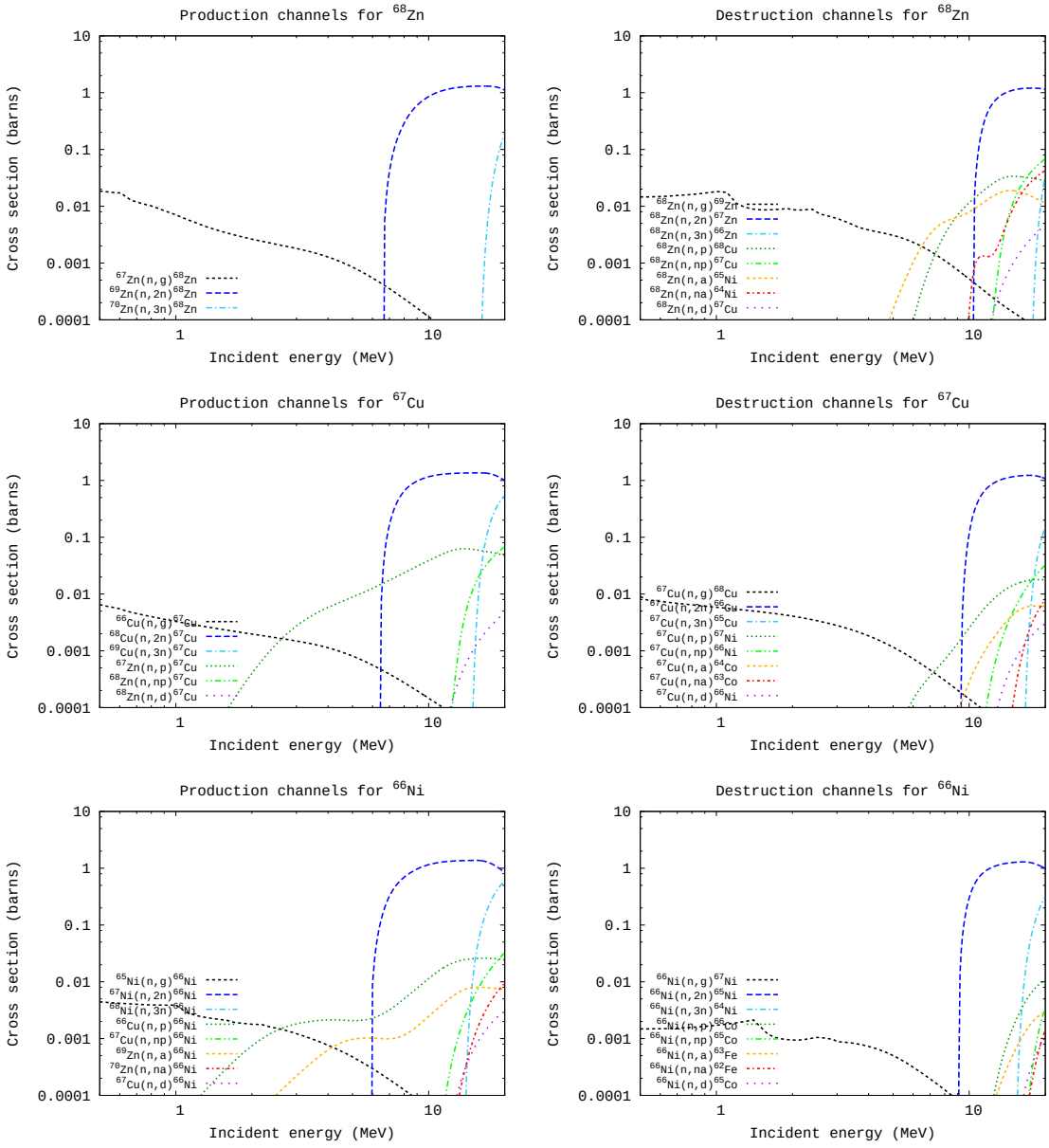

Fig. 12.— (continued)

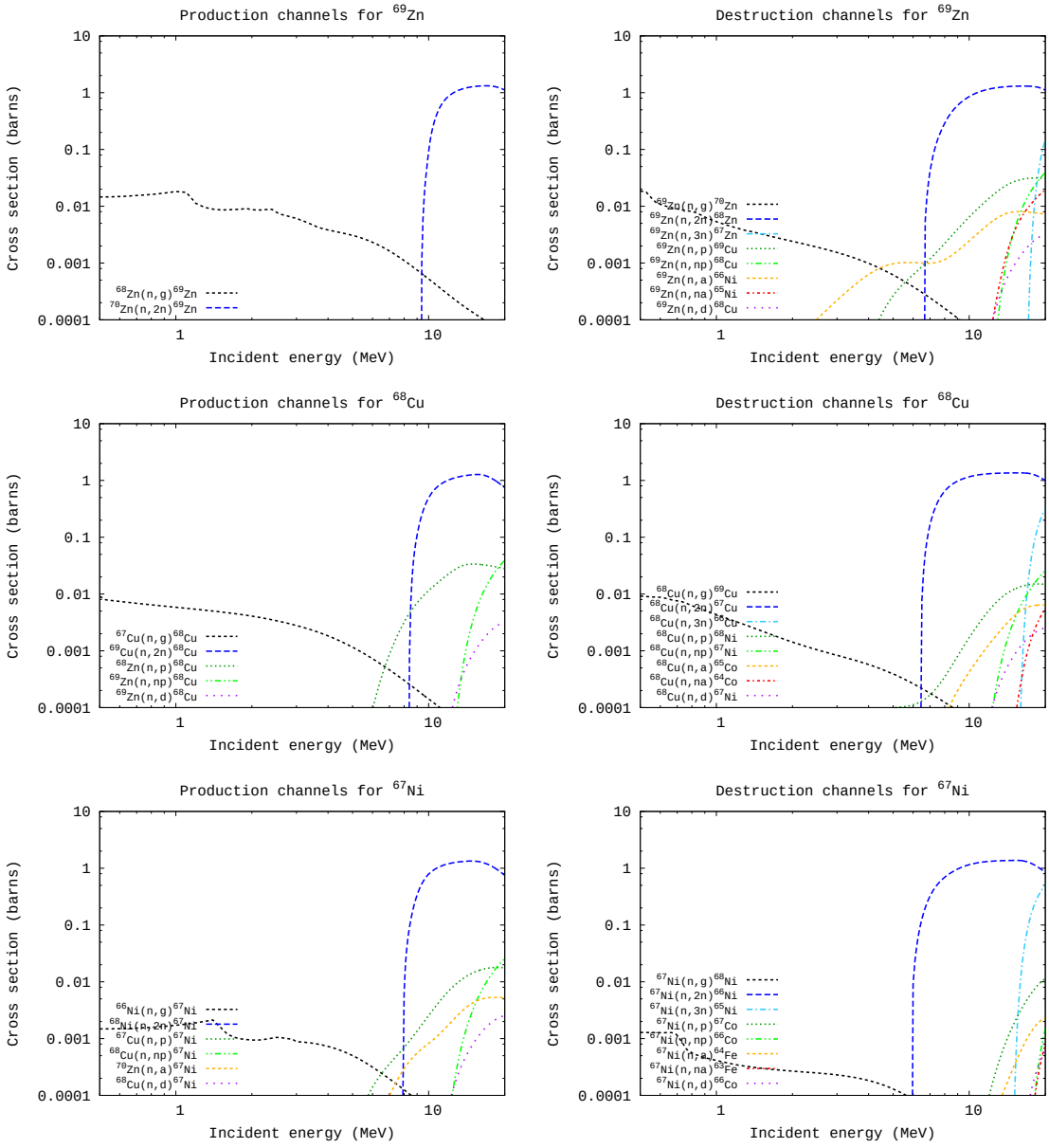

Fig. 12.— (continued)

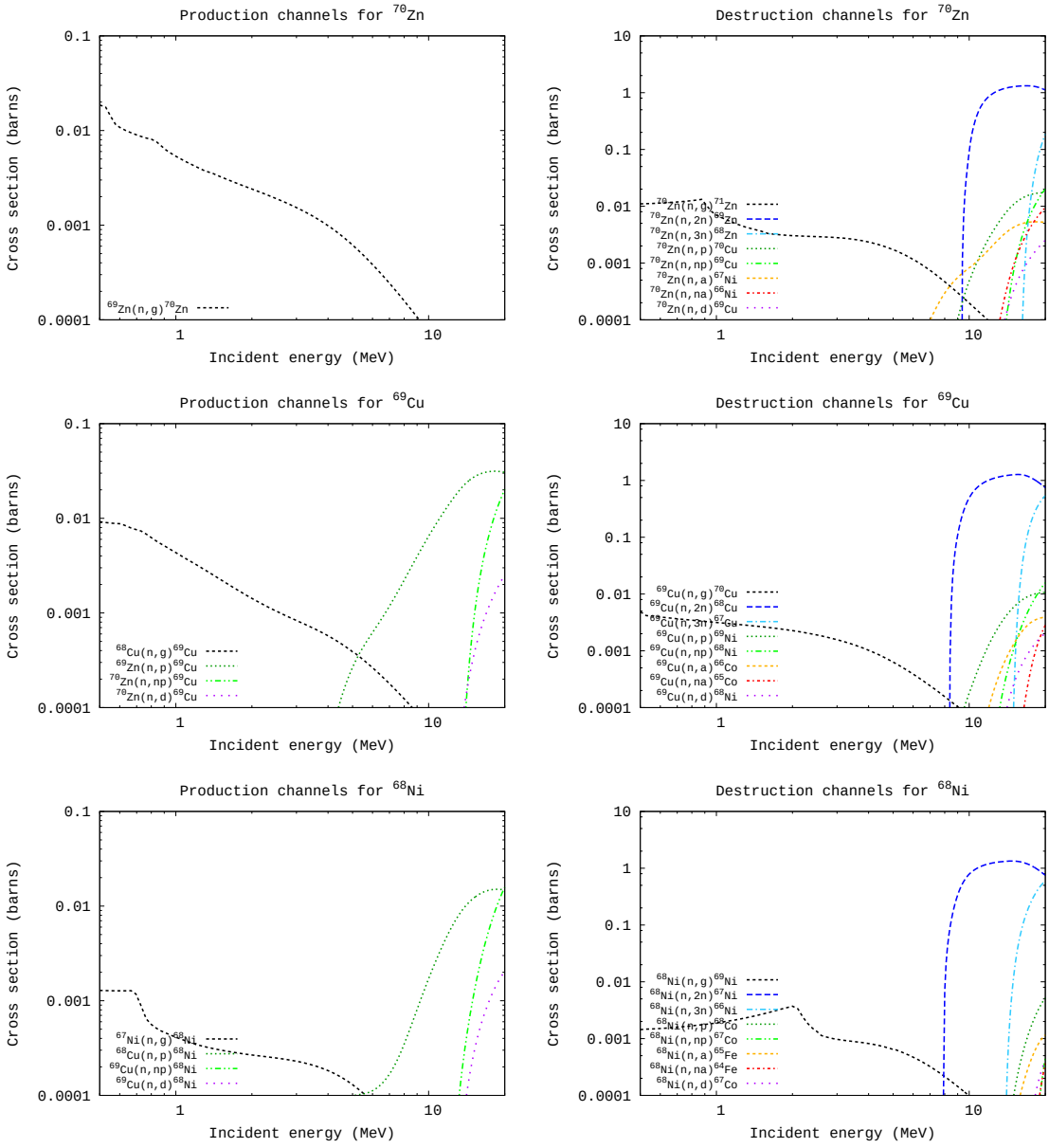

Fig. 12.— (continued)